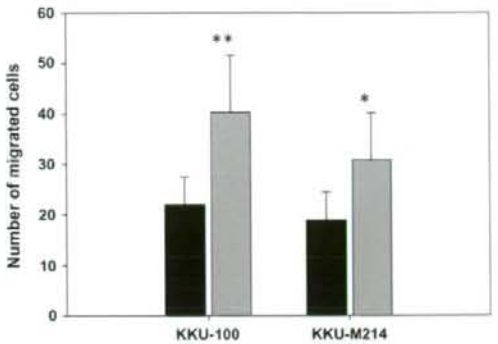

Fig. 5 – Effect of siGal-3 on cell motility. Numbers of migrated cells were compared between mock- (black bar) and siGal-3-treated CCA cells (grey bar). The data are the averaged values from triplicates and represent one of the two independent experiments. *P = 0.023, **P = 0.004.

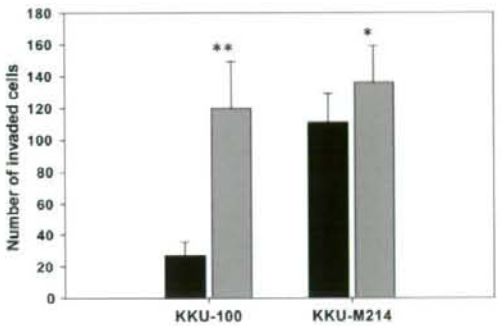

Fig. 6 – Effect of siGal-3 on cell invasion. The numbers of cells invading the Matrigel were compared between the mock- (black bar) and siGal-3-transfected CCA cells (grey bar). The data are the averaged values from triplicates and represent one of the two independent experiments. *P = 0.004; **P < 0.001.

nificantly enhanced cell migration and invasion in vitro, indicate that a decrease in Gal-3 expression may be an important factor influencing tumour progression in CCA. These results suggest that Gal-3 could be functionally involved in CCA progression and metastasis; however, further studies are necessary to detail the exact mechanism by which Gal-3 down-regulation influences the CCA phenotype.

Conflict of interest statement

None declared.

Acknowledgements

This project was co-supported by the Research Strengthening Grant 2006 from National Center for Genetic Engineering and Biotechnology (BIOTEC), National Science and Technology Development Agency (NSTDA); the Royal Golden Jubilee PhD Program (PHD/0140/2546 to Junking M. and Wongkham S.); and the Ministry of Education, Science and Culture of Japan (Araki N.) and JSPS-Asia Africa Science Platform Program (Khon Kaen University and Kumamoto University). We thank Mr. Bryan Roderick Hamman and Mr. Anthony Wayne Wilson for assistance with the English language presentation of this manuscript.

REFERENCES

1. Gray CA, Adelson DL, Bazer FW, Burghardt RC, Meeusen TE, Spencer TE. Discovery and characterization of an epithelial-specific galectin in the endometrium that forms crystals in the trophectoderm. *Proc Natl Acad Sci USA* 2004;101(21):7982–7.
2. Raz A, Zhu DG, Hogan V, et al. Evidence for the role of 34-kDa galactoside-binding lectin in transformation and metastasis. *Int J Cancer* 1990;46(5):871–7.
3. Castronovo V, Van Den Brule FA, Jackers P, et al. Decreased expression of galectin-3 is associated with progression of human breast cancer. *J Pathol* 1996;179(1):43–8.
4. Gong HC, Honjo Y, Nangia-Makker P, et al. The NH_2 terminus of galectin-3 governs cellular compartmentalization and functions in cancer cells. *Cancer Res* 1999;59(24):6239–45.
5. Ochieng J, Furtak V, Lukyanov P. Extracellular functions of galectin-3. *Glycoconj J* 2004;19(7–9):527–35.
6. Yu F, Finley Jr RL, Raz A, Kim HR. Galectin-3 translocates to the perinuclear membranes and inhibits cytochrome c release from the mitochondria. A role for synexin in galectin-3 translocation. *J Biol Chem* 2002;277(18):15819–27.
7. Takenaka Y, Fukumori T, Yoshii T, et al. Nuclear export of phosphorylated galectin-3 regulates its antiapoptotic activity in response to chemotherapeutic drugs. *Mol Cell Biol* 2004;24(10):4395–406.
8. Patterson RJ, Wang W, Wang JL. Understanding the biochemical activities of galectin-1 and galectin-3 in the nucleus. *Glycoconj J* 2004;19(7–9):499–506.
9. Shimura T, Takenaka Y, Tsutsumi S, Hogan V, Kikuchi A, Raz A. Galectin-3, a novel binding partner of beta-catenin. *Cancer Res* 2004;64(18):6363–7.
10. Sripa B, Kaewkes S, Sithithaworn P, et al. Liver fluke induces cholangiocarcinoma. *PLoS Med* 2007;4(7):e201.
11. Khan SA, Taylor-Robinson SD, Toledano MB, Beck A, Elliott P, Thomas HC. Changing international trends in mortality rates for liver, biliary and pancreatic tumours. *J Hepatol* 2002;37(6):806–13.
12. Thamavit W, Bhamarapravati N, Sahaphong S, Vajrasthira S, Angsubhakorn S. Effects of dimethylnitrosamine on induction of cholangiocarcinoma in *Opisthorchis viverrini*-infected Syrian golden hamsters. *Cancer Res* 1978;38(12):4634–9.
13. Vatanasapt V, Tangvoraphonkchai V, Titapant V, Pipitgool V, Viriyapap D, Sriamporn S. A high incidence of liver cancer in Khon Kaen Province, Thailand. *Southeast Asian J Trop Med Public Health* 1990;21(3):489–94.
14. Vatanasapt V, Uttaravichien T, Mairiang EO, Pairojkul C, Chartbanchachai W, Haswell-Elkins M. Cholangiocarcinoma in north-east Thailand. *Lancet* 1990;335(8681):116–7.
15. Sithithaworn P, Haswell-Elkins MR, Mairiang P, et al. Parasite-associated morbidity: liver fluke infection and bile duct cancer in northeast Thailand. *Int J Parasitol* 1994;24(6):833–43.

16. Brustmann H. Galectin-3 and CD1a-positive dendritic cells are involved in the development of an invasive phenotype in vulvar squamous lesions. *Int J Gynecol Pathol* 2006;25(1):30–7.
17. Song YK, Billiar TR, Lee YJ. Role of galectin-3 in breast cancer metastasis: involvement of nitric oxide. *Am J Pathol* 2002;160(3):1069–75.
18. Greene FL, Page DL, Fleming ID, et al. *AJCC cancer staging manual*. 6th ed. New York: Springer-Verlag; 2002.
19. Sripa B, Leungwattanawanit S, Nitta T, et al. Establishment and characterization of an opisthorchiasis-associated cholangiocarcinoma cell line (KKU-100). *World J Gastroenterol* 2005;11(22):3392–7.
20. Elbashir SM, Harborth J, Weber K, Tuschl T. Analysis of gene function in somatic mammalian cells using small interfering RNAs. *Methods* 2002;26(2):199–213.
21. Sawanyawisuth K, Wongkham C, Pairojkul C, et al. Methionine aminopeptidase 2 over-expressed in cholangiocarcinoma: potential for drug target. *Acta Oncol* 2007;46(3):378–85.
22. van den Brule F, Califice S, Castronovo V. Expression of galectins in cancer: a critical review. *Glycoconj J* 2004;19(7–9): 537–42.
23. Shimonishi T, Miyazaki K, Kono N, et al. Expression of endogenous galectin-1 and galectin-3 in intrahepatic cholangiocarcinoma. *Hum Pathol* 2001;32(3):302–10.
24. Su CH, Tsay SH, Wu CC, et al. Factors influencing postoperative morbidity, mortality, and survival after resection for hilar cholangiocarcinoma. *Ann Surg* 1996;223(4):384–94.
25. Kawarada Y, Yamagiwa K, Das BC. Analysis of the relationships between clinicopathologic factors and survival time in intrahepatic cholangiocarcinoma. *Am J Surg* 2002;183(6):679–85.
26. Lotz MM, Andrews Jr CW, Korzelius CA, et al. Decreased expression of Mac-2 (carbohydrate binding protein 35) and loss of its nuclear localization are associated with the neoplastic progression of colon carcinoma. *Proc Natl Acad Sci USA* 1993;90(8):3466–70.
27. van den Brule FA, Berchuck A, Bast RC, et al. Differential expression of the 67-kD laminin receptor and 31-kD human laminin-binding protein in human ovarian carcinomas. *Eur J Cancer* 1994;30A(8):1096–9.
28. Takano T, Miyauchi A, Yoshida H, Kuma K, Amino N. Decreased relative expression level of trefoil factor 3 mRNA to galectin-3 mRNA distinguishes thyroid follicular carcinoma from adenoma. *Cancer Lett* 2005;219(1):91–6.
29. Matarrese P, Tinari N, Semeraro ML, Natoli C, Iacobelli S, Malorni W. Galectin-3 overexpression protects from cell damage and death by influencing mitochondrial homeostasis. *FEBS Lett* 2000;473(3):311–5.
30. Califice S, Castronovo V, Bracke M, van den Brule F. Dual activities of galectin-3 in human prostate cancer: tumor suppression of nuclear galectin-3 vs tumor promotion of cytoplasmic galectin-3. *Oncogene* 2004;23(45):7527–36.
31. Honjo Y, Inohara H, Akahani S, et al. Expression of cytoplasmic galectin-3 as a prognostic marker in tongue carcinoma. *Clin Cancer Res* 2000;6(12):4635–40.
32. Goletz S, Hanisch FG, Karsten U. Novel alpha-GalNAc containing glycans on cytokeratins are recognized invitro by galectins with type II carbohydrate recognition domains. *J Cell Sci* 1997;110(Pt 14):1585–96.
33. Dumic J, Dabelic S, Flogel M. Galectin-3: an open-ended story. *Biochim Biophys Acta* 2006;1760(4):616–35.

THE JOURNAL OF BIOLOGICAL CHEMISTRY VOL. 283, NO. 14, pp. 9399–9413, April 4, 2008

Neurofibromatosis Type 1 (NF1) Tumor Suppressor, Neurofibromin, Regulates the Neuronal Differentiation of PC12 Cells via Its Associating Protein, CRMP-2*[S]

Received for publication, October 3, 2007, and in revised form, December 31, 2007 Published, JBC Papers in Press, January 23, 2008, DOI 10.1074/jbc.M708206200

Siriporn Patrakitkomjorn[‡], Daiki Kobayashi[‡], Takashi Morikawa[‡], Masayo Morifuji Wilson[‡], Nobuyuki Tsubota[‡], Atsushi Irie[§], Tatsuya Ozawa[‡], Masashi Aoki[‡], Nariko Arimura[¶], Kozo Kaibuchi[¶], Hideyuki Saya[‡], and Norie Araki[‡1]

From the [‡]Department of Tumor Genetics and Biology and [§]Department of Immunogenetics, Graduate School of Medical Sciences, Kumamoto University School of Medicine, Kumamoto 860-8556, and the [¶]Department of Cell Pharmacology, Nagoya University, Graduate School of Medicine, Nagoya, Aichi 466-8550, Japan

Neurofibromatosis type 1 (NF1) tumor suppressor gene product, neurofibromin, functions in part as a Ras-GAP, a negative regulator of Ras. Neurofibromin is implicated in the neuronal abnormality of NF1 patients; however, the precise cellular function of neurofibromin has yet to be clarified. Using proteomic strategies, we identified a set of neurofibromin-associating cellular proteins, including axon regulator CRMP-2 (Collapsin response mediator protein-2). CRMP-2 directly bound to the C-terminal domain of neurofibromin, and this association was regulated by the manner of CRMP-2 phosphorylation. In nerve growth factor-stimulated PC12 cells, neurofibromin and CRMP-2 co-localized particularly on the distal tips and branches of extended neurites. Suppression of neurofibromin using NF1 small interfering RNA significantly inhibited this neurite outgrowth and up-regulated a series of CRMP-2 phosphorylations by kinases identified as CDK5, GSK-3b, and Rho kinase. Overexpression of the NF1-RAS-GAP-related domain rescued these NF1 small interfering RNA-induced events. Our results suggest that neurofibromin regulates neuronal differentiation by performing one or more complementary roles. First, neurofibromin directly regulates CRMP-2 phosphorylation accessibility through the complex formation. Also, neurofibromin appears to indirectly regulate CRMP-2 activity by suppressing CRMP-2-phosphorylating kinase cascades via its Ras-GAP function. Our study demonstrates that the functional association of neurofibromin and CRMP-2 is essential for neuronal cell differentiation and that lack of expression or abnormal regulation of neurofibromin can result in impaired function of neuronal cells, which is likely a factor in NF1-related pathogenesis.

Neurofibromatosis type 1 (NF1)[2] is an autosomal dominantly inherited disorder, with an estimated prevalence of 1 in 3,000–4,000 people (1). The hallmarks of NF1 include development of benign tumors of the peripheral nervous system and an increased risk of developing malignancies. The phenotype of NF1 is highly variable, with several organ systems being affected, including the bones, skin, irises, and central and peripheral nervous systems. The effects on the nervous system manifest as neurofibroma, gliomas, and learning disabilities.

The *NF1* gene locates on chromosome 17q11.2 and encodes a large protein of 2,818 amino acids, neurofibromin (2). Because the great majority of *NF1* gene mutations frequently found in NF1 patients prevents the expression of intact neurofibromin, functional disruption of neurofibromin is potentially relevant to the expression of some or all of the multiple abnormalities that occur in NF1 patients (3).

A region centered around 360 amino acid residues encoded by the *NF1* gene shows significant homology to the known catalytic domains of mammalian Ras GTPase-activating protein (p120 GAP). This region is also similar to yeast IRA1/2 proteins, which have been shown to interact with Ras and mediate hydrolysis of Ras-bound GTP to GDP, resulting in inactivation of Ras protein function. The GAP-related domain of the *NF1* gene product (NF1-GRD) also stimulates Ras GTPase and consequently inactivates Ras protein (4–6). In the region of NF1-GRD, two different isoforms (type I and type II possessing higher and lower GAP activity, respectively) formed by alternative splicing have been identified (6).

Recently, we demonstrated a novel role for neurofibromin on neuronal differentiation in conjunction with regulation of Ras activity via its GAP-related domain (GRD) in NGF-stimulated PC12 cells serving as a model for neuronal cells (6). In PC12 cells, time-dependent increases in the GAP activity of cellular

* This work was supported by grants from, Cancer Research (to N. A.), Kiban Research (to N. A.), Houga Research (to N. A.) from the Ministry of Education, Science, and Culture of Japan (to N. A.), and from the Centers of Excellence Project B of Kumamoto University for proteomic research and education (to N. A.), from the Ministry of Health and Welfare of Japan (to H. S.), and from Japan Society for the Promotion of Science Asia and Africa Science Platform Program (to S. P. and N. A.). The costs of publication of this article were defrayed in part by the payment of page charges. This article must therefore be hereby marked "*advertisement*" in accordance with 18 U.S.C. Section 1734 solely to indicate this fact.

[S] The on-line version of this article (available at http://www.jbc.org) contains supplemental Movies 1 and 2 and Figs. S1–S5.

[1] To whom correspondence should be addressed: Dept. of Tumor Genetics and Biology, Graduate School of Medical Sciences, Kumamoto University, Kumamoto 860-8556, Japan. Tel.: 81-96-373-5323; Fax: 81-96-373-5120; E-mail: nori@gpo.kumamoto-u.ac.jp.

[2] The abbreviations used are: NF1, neurofibromin type 1; CRMP-2, collapsin response mediator protein-2; DN, dominant negative; GAP, GTPase-activating protein; GRD, GAP-related domain; siRNA, small interfering RNA; NGF, nerve growth factor; GST, glutathione *S*-transferase; CTD, C-terminal domain; CHAPS, 3-[(3-cholamidopropyl)dimethylammonio]-1-propanesulfonic acid; DTT, dithiothreitol; PBS, phosphate-buffered saline; PVDF, polyvinylidene difluoride; DIGE, difference gel electrophoresis; MS, mass spectrometry; MALDI-TOF, matrix-assisted laser desorption ionization time-of-flight; LC, liquid chromatography; ESI, electrospray ionization; CSRD, cysteine/serine-rich domain; FITC, fluorescein isothiocyanate; RhoK, Rho kinase.

neurofibromin (NF1-GAP) were detected after NGF stimulation, and these increases correlated with down-regulation of Ras activity during neurite elongation. Interestingly, the NF1-GAP increases were because of induction of alternative splicing of NF1-GRD type 1, which was triggered by NGF-induced Ras activation. Dominant-negative (DN) forms of NF1-GRD type I significantly inhibited the neurite extension of PC12 cells via regulation of the Ras state. NF1-GRD-DN also reduced axonal and dendritic branching/extension of rat embryonic hippocampal neurons. These results demonstrated that mutual regulation of Ras and NF1-GAP is essential for normal neuronal differentiation. Thus, we speculated that abnormal regulation of NF1-GAP in neuronal cells may be implicated in NF1-related learning and memory disorder (6). Recent studies using *Nf1* gene-targeting animals have also supported our hypothesis. For example, *Drosophila* homozygotes with *Nf1*-null mutation showed significant decrements in olfactory learning performance (4); *Nf1* heterozygous mice displayed spatial learning disability (7, 8), and mice lacking the alternatively spliced exon 23a of *Nf1* exhibited specific learning impairment (8). Furthermore, abnormal Ras activity in *Nf1* knock-out mice can disrupt learning and memory, indicating that the functional modulation of Ras by neurofibromin is essential for learning and memory.

To determine the precise cellular function of neurofibromin, we recently developed an acute knockdown system for neurofibromin using NF1-siRNAs, and we studied its effects on motility in several types of cell lines (9). In the glioma and HeLa cells, *NF1* siRNA treatment resulted in characteristic morphological changes such as abnormal actin stress fiber formation and elevated phosphorylation levels of cofilin, a protein that regulates actin cytoskeletal reorganization by depolymerizing and severing actin filaments. The elevated cofilin phosphorylation in neurofibromin-depleted cells was induced by activation of the Rho-RhoK/ROCK-LIMK2-cofilin pathway. Based on such evidence, we concluded that neurofibromin plays a significant role in actin cytoskeletal reorganization and cell motility (9).

The above observations prompted us to postulate that neurofibromin plays a key role in regulating cytoskeletal organization during axon formation or neurite outgrowth in neuronal cells, and that functional regulation by unknown factors associated with neurofibromin could collaborate in orchestrating these phenomena. The search for NF1-associated proteins is therefore of particular interest because it may both lead to the identification of novel cellular components in Ras-related and/or other pathways, as well as further our understanding of the mechanism of NF1-related pathogenesis.

In this study we analyzed the neurofibromin-associating proteins that functionally relate to neuronal cell differentiation. Using the newly established quantitative differential proteomic method, iTRAQ, more than 50 proteins were identified, including several neuronal regulating proteins. Out of the above, we focused on CRMP-2, which is known as a key molecule for axon formation and guidance. First, we observed that cellular colocalization of CRMP-2 and neurofibromin occurred especially on the neurites in NGF-treated PC12 cells. Subsequently, by suppressing neurofibromin expression using NF1 siRNA, we were able to analyze the functional association of CRMP-2 and neurofibromin in relation to the neurite outgrowth of PC12 cells. We observed that NF1 siRNA treatment resulted in up-regulation of a series of CRMP-2 phosphorylations and a significant inhibition of the neurite extension of NGF-treated PC12 cells. We then examined the functional correlation between CRMP-2 phosphorylation and neurofibromin suppression by analyzing specific related kinases in PC12 cells using unique proteomic strategies such as two-dimensional-DIGE combined with phosphoprotein staining and Western blotting using specific antibodies. Here we demonstrate that the neurofibromin function for neurite outgrowth of PC12 cells may involve the regulation of CRMP-2 phosphorylation via the direct interaction/complex formation with CRMP-2, and via the regulation of cellular CRMP-2 phosphorylating kinase cascades. We also discuss the implications of a functional association between neurofibromin and CRMP-2 for neuronal regulation in relation to NF1 pathogenesis.

EXPERIMENTAL PROCEDURES

Preparation of Glutathione S-transferase (GST) Fusion Proteins, Plasmid Constructions, and Transfections—GST fusion domain proteins of human neurofibromin corresponding to sequences of residues 543–909, 1168–1530, and 2260–2818 of neurofibromin, which were designated cysteine/serine-rich domain (CSRD), GAP-related domain (GRD), and C-terminal domain (CTD), respectively, were produced in *Escherichia coli* under the isopropyl 1-thio-β-D-galactopyranoside induction system and affinity-purified as described previously (10). Mammalian expression plasmids for NF1-GRD types 1 (pcDNA3-FLAG-GRD1X) were prepared as described previously (6). Human GST-CRMP2 plasmid construction and purification of GST-CRMP2 protein were performed as described previously (11). The GFP-NF1-CTD fusion protein expression vector was constructed by ligating KpnI/BamHI fragments of pAcGFP-C1 vector (Clontech) and pGEX-2TH/NF1-CTD (10). The vector was transfected to PC12 cells using Lipofectamine 2000 (Invitrogen) according to manufacturer's recommendation.

Antibodies and Inhibitors—An antibody against the C terminus of neurofibromin (anti-GRP (D)) was purchased from Santa Cruz Biotechnology (Santa Cruz, CA). The anti-human CRMP-2 (C4G) mouse IgG was purchased from IBL (Gunma, Japan). Monoclonal anti-α-tubulin (clone DM1A) and anti-β-tubulin (clone D66) were purchased from Sigma. The specific antibodies for phosphorylated CRMP-2, phospho-Thr^{514}, and phospho-Thr^{555} were prepared as described previously (12), and phospho-Ser^{522} was kindly provided from Dr. Y. Goshima (Yokohama City University). Secondary antibodies linked to horseradish peroxidase and Cy5 were purchased from Amersham Biosciences. Alexa Fluor® 488 goat anti-mouse IgG and Alexa Fluor® 568 goat anti-rabbit IgG were purchased from Invitrogen. Rhodamine phalloidin was purchased from Molecular Probes. ROCK inhibitor (Y27632), Cdk inhibitor (purvalanol A and olomoucine), and GSK-3β inhibitor (LiCl) were purchased from Calbiochem.

Purification of Binding Proteins from Mouse Brain Cytosolic Fraction by GST-CTD Affinity Chromatography—Mouse brain cytosolic fraction was prepared in lysis buffer A (20 mM Tris-

HCl, pH 7.5, 1 mM EDTA, 5 mM $MgCl_2$, 150 mM NaCl, and 0.1% Nonidet P-40) containing 1% protease inhibitors (mixture for mammalian tissues, Sigma) and 1 mM DTT, sodium fluoride (2 mM), sodium orthovanadate (2 mM), and okadaic acid (1 μM) as described (10). GST-CTD fusion proteins immobilized on GSH-agarose were packed onto a column and equilibrated with buffer B (30 mM Tris-HCl, pH 7.5, 1 mM EDTA, 5 mM $MgCl_2$, and 1 mM DTT). Mouse brain cytosolic fraction was pre-cleared by passing through a GSH column and then loaded onto the GST-CTD column or GST column as a control. After washing the column with buffer A, the proteins bound to the column were eluted by the addition of buffer C (buffer A containing 0.5 M NaCl) and used for the proteomic analysis. Protein concentrations of eluted samples were determined using the BCA protein assay (Pierce) or Bradford assay (Bio-Rad).

Silver Staining—Gels were fixed in fixative (50% methanol and 12% acetic acid) in 0.02% formaldehyde for at least 1 h. Gels were washed in 50% ethanol three times for 20 min and pretreated for 1 min by sodium thiosulfate (0.8 mM). Gels were rinsed in distilled water three times for 20 s. Silver nitrate solution (0.2%) in 0.03% formaldehyde was used for impregnating for 20 min, following rinsing with distilled water two times for 20 s. Developing solution (0.7 M of sodium carbonate, 0.02% formaldehyde, and 16 μM of sodium thiosulfate) was used for developing. Gels were rinsed two times in distilled water for 2 min. Stopping solution (50% methanol and 12% acetic acid) was used for stopping the reaction, and gels were kept in 50% methanol.

iTRAQ Sample Preparation and Quantitative Analysis—The 200 μl of protein samples (100 μg) were precipitated with 6× volume of acetone and kept overnight at −80 °C. After centrifugation of the samples at 13,000 × *g* for 5 min, the precipitants were kept and dissolved in 200 μl of 50 mM NH_4HCO_3, 2 mM $CaCl_2$, and 10% AcCN; then 1 μg of trypsin (Promega) was added and incubated at 37 °C for 2 h. Another 1 μg of trypsin was added before incubating overnight, after which the samples were kept at −80 °C until analysis. Samples were labeled with iTRAQ tags as follows: 100 μg of duplicated protein trypsin peptide fractions eluted from the GST-CTD column were labeled with iTRAQ116 and iTRAQ117; 100 μg of duplicated fractions from GST column as controls were labeled with iTRAQ114 and -115. The labeled samples were then all mixed, desalted, and subjected to LC-ESI-QQ-TOF and LC-MALDI-TOF-TOF MS analysis using the UltiMate NanoLC system (LCPackings A Dionex Company), the API QSTAR Pulsar i, or the 4700 Proteomics analyzer (Applied Biosystems). Obtained data were processed with iTRAQ quantitative analysis software ProQuant version 1.1 for ESI-QQ-TOF MS or GPS Explorer version 3.1 for MALDI-TOF-TOF MS (Applied Biosystems) and MASCOT (Matrix Science).

Immunoprecipitation Assays—Mouse brain was homogenized with lysis buffer A containing 1% protease inhibitor mixture for mammalian tissues (Sigma) and 1 mM DTT, sodium fluoride (2 mM), sodium orthovanadate (2 mM), and okadaic acid (1 μM) as the phosphatase inhibitors. Samples were centrifuged at 10,000 rpm for 10 min, and the supernatants were mixed with the indicated antibodies for 3 h and then mixed with appropriate protein A or G-Sepharose 4 Fast Flow beads (GE Healthcare) for 1 h. The beads were washed with buffer A, and boiled in 2× SDS loading buffer. Samples were separated by SDS-PAGE, transferred into PVDF membrane electrophoretically, and subjected to immunoblotting analysis with the indicated antibodies. After reaction with horseradish peroxidase- or Cy5-conjugated secondary antibodies, the reacted protein pattern on the membrane was visualized by an ECL detection system or by scanning with fluorescent scanner Typhoon 9400 (GE Healthcare), respectively.

Binding Assay of CRMP-2 to Neurofibromin Fragments in Vitro—The GST fusion neurofibromin fragment proteins (GST-CSRD-(543–909), GST-GRD-(1168–1530), GST-CTD-(2260–2818)), or GST (500 μg) purified from *E. coli* were immobilized on GSH-agarose beads and packed onto columns. CRMP-2 protein (500 μg) was prepared after the thrombin (48 units) treatment of GST-CRMP-2 in thrombin cleavage buffer (50 mM Tris-HCl, pH 8.8, 150 mM NaCl, 2.5 mM $CaCl_2$) for 40 min at room temperature, followed by the gel filtration. Purified CRMP-2 was applied to the neurofibromin fragment columns and washed with buffer A, and the bound CRMP-2 on each column was eluted by 2× SDS loading buffer. The eluted fractions were separated by SDS-PAGE, transferred onto PVDF membrane electrophoretically, and subjected to the immunoblotting analysis with anti-CRMP-2 antibody. To check the purity of thrombin-cleaved CRMP-2 and GST-neurofibromin fragments (GST-CSRD, -GRD, -CTD), each protein was subjected to SDS-PAGE and their patterns analyzed after staining with Simply Blue (Fig. 1*D*, *upper panel*).

Quantitative Western Blotting Analysis—After immunoblotting detection, the ECL patterns were scanned using LabScan 5.0 (GE Healthcare) with transparent mode and resolution 300 dpi, and Cy5 patterns were processed by fluorescence scanner Typhoon 9400. The intensities were measured using ProGenesis Work station version 2005 (PerkinElmer Life Sciences) or ImageQuant (GE Healthcare) with background subtraction and normalization by total spot volume mode. The intensity of each spot was recorded as digital data, and processed by Microsoft Office Excel. Experimental values are expressed as mean ± S.E. Paired Student's *t* test or one-way analysis of variance with Dunnett's test was used to identify significant differences where appropriate. *p* values of <0.05 were considered significant.

Cell Culture, Stimulation, Transfection, and Preparation of Cell Lysates—PC12 cells were cultured under 5% CO_2 at 37 °C in Dulbecco's modified Eagle's medium (Invitrogen) supplemented with 10% horse serum and 5% fetal bovine serum. Transfection into cells was performed with Lipofectamine 2000 (Invitrogen) according to the manufacturer's protocol. PC12 cells were stimulated with 50 ng/ml 2.5 S NGF (WAKO) for up to 72 h. For preparation of cellular lysates, cells were solubilized with NF1 lysis buffer (20 mM Tris-HCl, pH 7.5, 5 mM $MgCl_2$, 150 mM NaCl, 1 mM EDTA, 0.1% Nonidet P-40, 1 mM 4-(2-aminoethyl)-benzenesulfonyl fluoride hydrochloride, 1 μg/ml each aprotinin, pepstatin A, and leupeptin) and passed through a 25-gauge syringe 20 times. Lysates were centrifuged at 20,000 × *g* for 20 min at 4 °C, and the protein concentrations of

the supernatants were determined using the BCA protein assay (Pierce).

siRNA—Four target sequences for Rat NF1 siRNA were designed as follows: a 21-oligonucleotide siRNA duplex was designed as recommended elsewhere (9) and was synthesized by Gene Link (Japan) to target the rat NF1 sequence 5′-^{249}CAAGGAGTGTCTGATCAACTT-3′ (for 249 NF1 siRNA), sequence 5′-^{532}CTTCGGAATTCTGCTTCTGTT-3′ (for 532 NF1 siRNA), and sequence 5′-^{611}GGTTACAGGAGT-TGACTGTTT-3′ (for 611 NF1 siRNA). Annealing of the component strands of each siRNA and transfection were performed as described (9). FITC-labeled rat NF1 sequence (FITC-249 NF1 siRNA) was also synthesized by Gene Link. A 27-oligonucleotide siRNA duplex was designed and synthesized by iGENE therapeutics (Japan) to target the rat NF1 sequence 5′-GAAAGGGGCUUGAAGUUAAUGUCAAAG-3′. For control siRNAs, a 27-oligonucleotide siRNA duplex scramble sequence by iGENE therapeutics (Japan), and a double-stranded RNA targeting human *NF1* gene (5′-^{609}AACTTCG-GAATTCTGCCTCTG^{629}-3′) were used as a control.

Immunofluorescence Analysis—PC12 cells grown on a 35-mm culture dish were fixed with 4% paraformaldehyde in PBS for 15 min at room temperature and then permeabilized with 0.2% Triton X-100 in PBS for 15 min. After being washed with PBS, cells were incubated in primary antibodies diluted in PBS containing 0.2% bovine serum albumin, followed by a secondary antibody conjugated with a fluorescent dye for 60 min at room temperature, or the cells were incubated with rhodamine phalloidin to stain cellular actin for 60 min at room temperature. Analysis was performed with a confocal microscope (Fluoview, FV300, Olympus) or fluorescence microscope (with 20 × 1.6 Olympus IX71) (DPController, DPManager).

Time-lapse Video Analysis—Cells were placed on a collagen-coated glass-bottom plate with 6 wells (Iwaki). Dishes were maintained at 37 °C under 5% CO_2 in the chamber set under the camera, during the observation. Images were obtained using a 20× UPlan Apo objective (Olympus). The camera, shutters, and filter wheel were controlled by MetaMorph imaging software (Universal Imaging), and the images were collected every 5 min with exposure times of 100 ms. Through-focus z-series stacks consisting of three frames were acquired at each time point.

Two-dimensional Electrophoresis and Two-dimensional Difference Gel Electrophoresis (DIGE)—Mouse brain or PC12 cell lysates (10–50 μg), after desalting using two-dimensional-clean up kit (Amersham Biosciences), were mixed with 125 μl of rehydration solution (8 M urea, 0.5% (w/v) CHAPS, 0.2% (w/v) DTT, 0.5% (v/v) IPG buffer) and loaded into strip holders for first-dimension isoelectric focusing. IPG strips (pH 4–7) (Amersham Biosciences) were used and allowed to re-swell for 12 h. Strips were equilibrated in a two-step process in equilibration solution (2% SDS, 50 mM Tris-HCl, pH 8.8, 6 M of urea, 30% (v/v) glycerol, and 0.002% bromphenol blue) for 15 min each step. In step one, 1 mM DTT was added; in step two, 1 mM iodoacetamide was added. Strips were then subjected to two-dimensional SDS-PAGE (10% gel, 7 × 7 or 13 × 13 cm^2). The proteins separated in two-dimensional gels were stained with protein staining solutions or transferred onto nitrocellulose or PVDF membranes, and protein patterns were obtained using specific antibodies. The two-dimensional pattern images on the gels or membranes were visualized with fluorescence probes or ECL (GE Healthcare) and scanned by a confocal fluorescence scanner Typhoon 9400 (GE Healthcare).

For two-dimensional DIGE, mouse brain or PC12 cell lysates (10–50 μg) were labeled with 400 pmol of CyDye DIGE Fluor minimal dyes (GE Healthcare) freshly dissolved in anhydrous dimethylformamide. The labeling mixture was incubated on ice in the dark for 30 min, and the reaction was terminated by addition of 10 nmol of lysine. Equal volumes of 2× sample buffer (8 M urea, 4% (w/v) CHAPS, 2 mg/ml DTT, 1% (v/v) IPG buffer, pH 4–7) were added to each of the labeled protein samples. The two samples were mixed prior to isoelectric focusing by IPG strip and subjected to the two-dimensional PAGE as described above.

Staining of the Two-dimensional Gels by ProQuant Diamond Phosphoprotein Gel Stain and SYPRO Ruby Protein Gel Stain—For ProQuant Diamond staining, two-dimensional gels were fixed in 50% methanol containing 10% acetic acid once for 30 min and again for overnight. Gels were washed three times in water for 10 min and stained with ProQuant Diamond phosphoprotein gel stain (Invitrogen) in the dark for 60–90 min and then washed with destain solution (5% of 1 M sodium acetate, pH 4.0, containing 20% acetonitrile) three times for 30 min. Gels were washed twice with water for 5 min and scanned by Typhoon. For SYPRO Ruby gel staining, gels were fixed in 50% methanol containing 7% acetic acid for 30 min, stained in SYPRO Ruby protein gel stain (Invitrogen) for 3 h, and washed with 10% methanol containing 10% acetic acid for 30 min. The fluorescent images were scanned with Typhoon 9400, visualized, and processed as digital data with data mining software ImageQuant version 5.2, DeCyder (GE Healthcare), and ProGenesis Work station version 2005 (PerkinElmer Life Sciences).

RESULTS

The Identification of Neurofibromin C-terminal Associating Proteins—To isolate proteins that physically associate with neurofibromin, we used the C-terminal domain (CTD), one of the crucial regions in regulating neurofibromin function (10, 14), as a ligand. Mouse brain cytosolic lysates were loaded onto the affinity column with immobilized GST-CTD or GST. Associating proteins on both columns were eluted using high salt elution buffer. The concentration of eluted protein from the GST-CTD column was 3.7 times higher than that from the control column (Fig. 1*A*). To subject the proteins eluted from each column to iTRAQ analysis, each fraction was adjusted to the same protein concentration, separately trypsinized, and modified with four kinds of isobaric tags as follows: iTRAQ114 and -115 for control and iTRAQ116 and -117 for NF1-binding proteins. Four fractions modified with different iTRAQ tags were combined and subjected to NanoLC ESI QQTOF and NanoLC-MALDI-TOF-TOF analysis. The obtained MS/MS data were used for the identification of the specific CTD-associating proteins, and the iTRAQ tag ratio (116, 117 *versus* 114, 115) was calculated using ProQuant quantitatively.

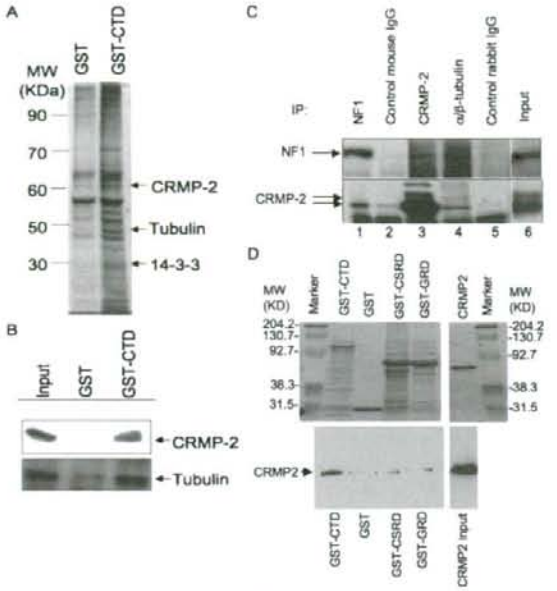

FIGURE 1. **Identification of neurofibromin-associating proteins.** *A*, silver staining of the associating proteins for the C-terminal domain of neurofibromin (GST-CTD) or those for the control (GST). Mouse brain proteins bound to the immobilized GST or GST-CTD are separated by SDS-PAGE and visualized with silver staining as described under "Experimental Procedures." The molecular mass markers are shown in kDa on the *left*, and *arrows* indicate the positions of the specific binding proteins identified. *B*, Western blotting analysis of identified proteins by the antibodies against CRMP-2 and tubulin. The eluted fraction from mouse brain proteins bound to immobilized GST or GST-CTD was immunoblotted with anti-CRMP-2 antibodies and anti-α-tubulin antibodies, followed by visualization with the ECL detection system. *C*, immunoprecipitation (*IP*) analysis of CRMP-2, tubulin α/β, and neurofibromin. Extracts of mouse brain in lysis buffer were incubated with anti-neurofibromin (*lane 1*), anti-CRMP-2 (*lane 3*), anti-tubulin α/β (*lane 4*) antibodies, and control anti-rabbit (*lane 2*) or mouse (*lane 5*) IgG antibodies for 3 h at 4 °C. The immunoprecipitates were analyzed by immunoblotting using the indicated antibodies (*upper panel*, anti-neurofibromin antibody; *lower panel*, anti-CRMP2 antibody) as described under "Experimental Procedures." *Input* (*lane 6*) shows the supernatant of the extract of mouse brain used for this study. *Arrows* indicate the position of the protein for neurofibromin (NF1) and CRMP-2 (*upper arrow*, phosphorylated form; *lower arrow*, nonphosphorylated form). *D*, direct binding of CRMP-2 to neurofibromin fragments *in vitro*. The GST fusion neurofibromin fragment proteins (GST-CSRD-(543–909), GST-GRD-(1168–1530), GST-CTD-(2260–2818)), GST, and CRMP2 (10 μg) purified from *E. coli* were separated with SDS-PAGE and stained with Coomassie Brilliant Blue (*upper panel*). Each of the GST fusion proteins (GST-CSRD, GST-GRD, and GST-CTD) and GST were immobilized on GSH-agarose beads and packed into each columns. Purified CRMP-2 protein (*upper panel, right photo*) was applied to the neurofibromin fragment columns and washed with buffer *A*, and the bound CRMP-2 on each column was eluted, subjected to SDS-PAGE (10%), and analyzed with Western blotting using anti-CRMP-2 antibody (*lower panel*) as described under "Experimental Procedures." The molecular mass markers are shown in kDa on the *left* and *right* in the *upper panel*, and an *arrow* indicates the positions of CRMP-2 identified in Western blotting.

At least 58 proteins having a specific high ratio of affinity to the GST-CTD compared with the GST column (an identification total ion score more than 61 and the best ion score confidence interval % more than 97%) were listed in Table 1. Identified proteins include not only the proteins previously found, such as neurofibromin-associating proteins 14-3-3s (14) and tubulins (13), but also many novel proteins not reported previously. The proteins were categorized into five main groups by their following biological functions: 1) cytoskeleton and its regulators, ARP2/3 complex 20-kDa subunit, actins, tubulins, and cofilin; 2) axonal outgrowth and guidance, collapsin-response mediator protein-2, CRMP-2/dihydropyrimidinase-related protein-2, and DRP-2, DRP-1; 3) neurotransmitter secretion, synapsin I and synaptojanin 1; 4) endocytosis, dynamin-1, protein kinase C, and casein kinase substrate in neurons protein 1; and 5) transcription translation regulator, EF1-α2, -γ, transcriptional activator protein PUR-α, SET protein, nucleosome assembly protein 1-like 1, and so on. Consistent with our interest in the function of neuronal cellular regulation associated to NF1 pathogenesis (6), we focused on CRMP-2, which showed one of the most significant associations in the GST-CTD column compared with those of control GST (Table 1).

To confirm that CRMP-2 is a neurofibromin-associating protein, the binding fractions of GST-CTD and control GST were separated by SDS-PAGE (10% polyacrylamide gel) and analyzed with silver staining (Fig. 1*A*) or immunoblotting using anti-CRMP-2 antibodies (Fig. 1*B*). CRMP-2 was significantly identified in the GST-CTD associating-protein fraction, although it was not obvious in that of the control GST fraction. Using the iTRAQ processing method, we detected 2.4 times higher CRMP-2 binding affinity (8.88 times higher CRMP-2 binding affinity: the ratio compensated with protein concentrations recovered from each column) in the GST-CTD fraction compared with the control GST fraction. The total ion score of identified 18 CRMP-2 peptides was 1437.

CRMP-2 and Tubulin Form a Complex with Neurofibromin in Vivo—CRMP-2, a tubulin-binding protein, has been known as a key molecule for axon guidance and is thought to form a protein complex whose effects on the regulation of microtubule formation in neuronal cells have not been completely identified (11). To confirm the association of CRMP-2 and tubulin to neurofibromin *in vivo*, the immunoprecipitates of the brain cytoplasmic protein fraction with antibodies against tubulin α and β, CRMP-2, and neurofibromin were analyzed by Western blotting (Fig. 1*C*). The interaction of tubulin was strong with the nonphosphorylated form of CRMP-2 (lower band for CRMP-2 in Fig. 1*C*), which is an active form and is increased in the intensity by the absence of phosphatase inhibitors, as reported (11), Interestingly, the binding of nonphosphorylated CRMP-2 to neurofibromin was significantly stronger than that of phosphorylated CRMP-2 (Fig. 1*C*). These results suggested that nonphosphorylated CRMP-2 forms a complex with neurofibromin as well as tubulin.

CRMP-2 Directly Binds to Neurofibromin C-terminal Domain—To analyze whether CRMP-2 binds directly to the neurofibromin or not, *in vitro* pulldown assay was performed with using recombinant CRMP-2 and GST-neurofibromin N-terminal center and C-terminal domain fragments. GST-CSRD-(543–909), GST-GRD-(1168–1530), GST-CTD-(2260–2818), or GST were immobilized on GSH-agarose beads and packed onto columns, and CRMP-2 protein was applied to each column. The bound CRMP-2 on each column was eluted and subjected to the Western blotting analysis using anti-CRMP-2 antibody. As shown in Fig. 1*D*, *lower panel*, CRMP-2 was detected in the eluates only from the GST-CTD column, suggesting that CRMP-2 could bind directly to the neurofibro-

TABLE 1
Neurofibromin-binding proteins identified with iTRAQ method

Protein name	Mass in Da	Peptide count[a]	Total ion score[b]	Best ion score C.I.[c] %	iTRAQ ratio average	S.E.[d]	Accession no.
Dihydropyrimidinase-related protein-2 (collapsin-response mediator protein 2 (CRMP-2))	67,393	18	1437	100	2.4	0.2	P47942
Nucleosome assembly protein 1-like	51,191	2	77	99.9	7.5	1.9	Q9Z2G8
Transcriptional activator protein PUR-α	38,003	5	331	100	6.4	0.9	P42669
Complement component 1, Q subcomponent binding protein, mitochondrial precursor	33,929	2	143	100	5.4	0.7	O35658
SET protein	36,844	3	247	100	5.3	0.7	Q63945
60 S ribosomal protein L22	17,558	2	85	100	4.3	0.9	P41104
Adapter-related protein complex 2 β1 subunit	114,363	2	74	99.9	3.5	1.4	Q9DBG3
Tubulin β chain	52,693	6	387	100	3.3	0.3	P04691
Tubulin β4 chain	52,138	4	322	100	3.2	0.4	Q9D6F9
Elongation factor 1-α	57,537	4	195	100	3.2	0.6	P62632
Tubulin α-2 chain	53,700	10	657	100	3.0	0.5	P05213
Synapsin I	74,486	4	201	100	2.9	0.8	O88935
Synaptojanin 1	186,358	2	135	100	2.8	0.6	Q8CHC4
Dynamin-1	106,354	3	141	100	2.8	0.3	P39053
Elongation factor 1-γ	55,271	4	164	100	2.8	0.7	Q9D8N0
Clathrin coat assembly protein AP180	99,365	2	68	99.9	2.7	0.5	Q05140
Hydroxyacylglutathione hydrolase (glyoxalase II)	32,482	2	115	100	2.7	0.8	Q99KB8
Guanine nucleotide-binding protein G(o), α subunit 1	44,389	2	74	99.9	2.5	0.3	P18872
Transcription factor A, mitochondrial precursor	33,008	2	62	99.7	2.5	0.3	Q91ZW1
Succinate semialdehyde dehydrogenase	57,424	2	89	100	2.5	0.7	P51650
Hexokinase, type I	118,767	4	168	100	2.5	0.4	P17710
Myelin basic protein	29,601	6	380	100	2.5	0.6	P04370
Transitional endoplasmic reticulum ATPase	96,894	2	79	100	2.4	0.2	P46462
Keratin, type I cytoskeletal 10	61,017	4	218	100	2.4	0.3	P02535
Microtubule-associated protein tau	87,172	2	108	100	2.3	0.4	P19332
Heat shock protein HSP 90-β (HSP 84)	94,427	8	519	100	2.3	0.3	P34058
Fumarate hydratase, mitochondrial precursor	59,614	2	131	100	2.3	0.5	P14408
Heat shock cognate 71-kDa protein	78,981	17	1092	100	2.3	0.2	P63018
Dihydropyrimidinase related protein-1 (Collapsin-response mediator protein 1 (CRMP-1))	67,542	3	384	100	2.3	0.5	Q62950
Actin, cytoplasmic 1 (β-actin)	44,934	9	526	100	2.3	0.1	P60710
Glyceraldehyde-3-phosphate dehydrogenase (GAPDH)	40,002	3	264	100	2.3	0.6	P04797
Heat shock protein HSP 90-α (HSP 86)	96,675	3	507	100	2.3	0.3	P07901
Nucleoside diphosphate kinase B	19,259	2	83	100	2.3	0.6	P19804
Malate dehydrogenase, mitochondrial precursor	39,632	3	155	100	2.3	0.2	P08249
Hemoglobin α chain	16,731	5	218	100	2.2	0.4	P01942
Protein kinase C and casein kinase substrate in neurons protein 1	57,082	4	226	100	2.2	0.2	Q61644
Serine/threonine protein phosphatase 2A, catalytic subunit, β isoform	37,852	2	76	99.9	2.1	0.3	P62715
Vacuolar protein sorting 35	99,082	2	141	100	2.1	0.4	Q9EQH3
Stress-70 protein, mitochondrial precursor	81,549	2	75	100	2.1	0.4	P38647
SH3-containing GRB2-like protein 2	44,202	4	330	100	2.1	0.3	Q62420
ARP2/3 complex 20 kDa	21,786	2	61	97.9	2.1	0.4	P59999
Glutamine synthetase	45,829	6	353	100	2.0	0.2	P15105
Hemoglobin β-1 chain	17,542	4	279	100	2.0	0.2	P02088
Osmotic stress protein 94	105,985	3	197	100	2.0	0.2	P48722
Aspartate aminotransferase, mitochondrial precursor	52,248	2	138	100	2.0	0.4	P05202
L-Lactate dehydrogenase A chain	40,721	4	270	100	1.8	0.3	P06151
Malate dehydrogenase, cytoplasmic	40,961	5	342	100	1.8	0.1	P14152
Aldehyde dehydrogenase, mitochondrial precursor	61,482	5	284	100	1.8	0.2	P47738
Creatine kinase, ubiquitous mitochondrial precursor	50,111	3	252	100	1.7	0.2	P30275
Ubiquitin-activating enzyme E1	126,857	3	141	100	1.7	0.7	Q02053
78-kDa glucose-regulated protein precursor	81,426	4	165	100	1.7	0.1	P20029
Heat shock 70-related protein APG-2	106,832	8	484	100	1.7	0.1	Q61316
Ferritin heavy chain	23,111	2	88	100	1.7	0.2	P09528
14-3-3 protein β/α	31,046	2	523	100	1.7	0.2	P35213
14-3-3 protein ε	32,064	5	407	100	1.7	0.1	P62260
4-Aminobutyrate aminotransferase, mitochondrial precursor (GABA aminotransferase)	61,567	2	87	100	1.7	0.1	P61922
Aspartate aminotransferase, cytoplasmic	49,383	5	250	100	1.7	0.1	P05201
Glutamate dehydrogenase, mitochondrial precursor	66,775	11	631	100	1.6	0.1	P10860

[a] Peptide count represents number of peptides using iTRAQ quantitation.
[b] Total ion score represents confidences of protein identification.
[c] Best ion score C.I. % represents confidences of protein identification and MS/MS spectrum.
[d] S.E. represents standard error of iTRAQ ratio average.

min C-terminal domain without intermediate proteins such as tubulin or other binding proteins that were identified in this study.

Neurofibromin Is Co-localized with CRMP-2 in the Distal Tips of Neurites in Differentiated PC12 Cells—To demonstrate the localization of neurofibromin in differentiated PC12 cells, after NGF treatment of the cells we examined the expression pattern of neurofibromin immunocytochemically using anti-NF1 antibody. As shown in Fig. 2, neurofibromin was significantly distributed throughout the cells, being found in the perinucleus, the cytoplasm, and the apical region of neurites (Fig. 2*A*). To further confirm the co-localization of neurofibromin and CRMP-2 in differentiated PC12 cells, we analyzed the expression patterns of both CRMP-2 and neurofibromin using both anti-NF1 and anti-CRMP-2 antibodies. As we expected, CRMP-2 was found to be co-localized with neurofibromin in

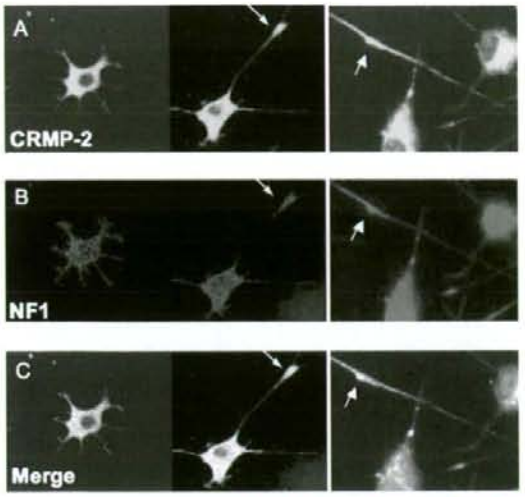

FIGURE 2. **Co-localization of neurofibromin and CRMP-2 in differentiated PC12 cells.** PC12 cells with NGF stimulation were detected by rabbit anti-NF1 (4 μg/ml) (*B* and *C*) and mouse anti-CRMP-2 antibodies (5 μg/ml) (*A* and *C*), and followed by Alexa 568-conjugated anti-rabbit IgG antibody (*red*), and Alexa 488-conjugated anti-mouse antibody (*green*), respectively, as described under "Experimental Procedures." The co-localization was shown in the merged image (*C*) with *yellow color*. Cells were observed by a confocal microscope (Fluoview, FV300, Olympus) or fluorescence microscope (with 20 × 1.6 OLYMPUS IX71) (DPController, DPManager). The *arrows* point to regions of neurofibromin and CRMP-2 co-localization in the distal tips and branches along the neurites. The results were reproducible in five experiments performed with independent preparations.

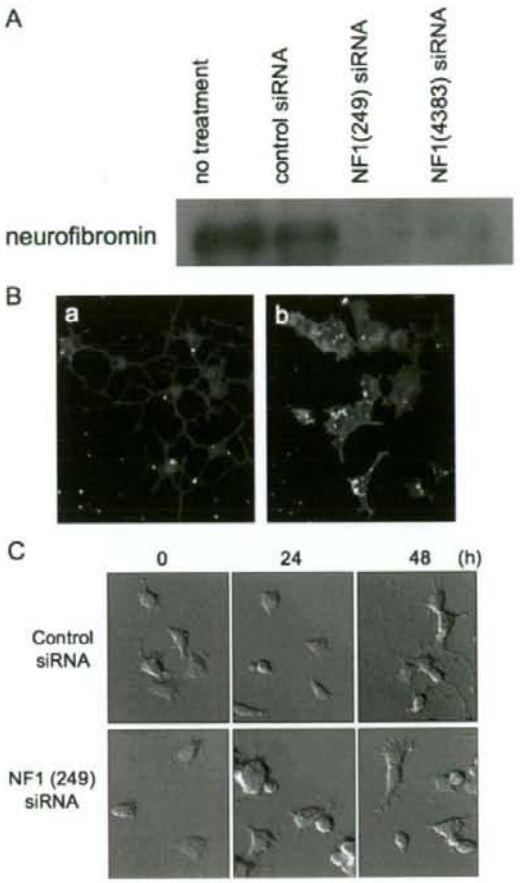

FIGURE 3. **Effects of the NF1 siRNA on neurite outgrowth of PC12 cells.** *A*, immunoblot analysis of whole cell lysates extracted from PC12 cells, transfected with siRNA for NF1(249), NF1(4383), or control siRNA. Cells were harvested after 48 h of NF1 siRNA or control siRNA transfection and analyzed by immunoblotting with the anti-neurofibromin antibodies. *B*, suppression of NF1 expression leads to changes in neurite outgrowth of PC12 cells. Cells were fixed and reacted with rhodamine phalloidin to stain actins after 48 h of transfection of FITC-NF1(249) siRNA, and observed with the confocal fluorescent microscope. The *red fluorescence* shows actin dynamics, and the *green* or *yellow fluorescences* (merged with actin) show FITC-NF1 siRNA incorporated into the perinuclear space with a specific manner (*b*) or attached on the cellular surface with nonspecific manner (*a*). *C*, representative images of time-lapse video analysis of PC12 cells transfected with NF1 siRNA or control siRNA; PC12 cells were transfected with NF1(249) siRNA or control siRNA, stimulated with NGF, and analyzed by time-lapse. The images show the morphology of PC12 cells transfected with NF1 siRNA (*lower panel*) or control siRNA (*upper panel*) at 0, 24, and 48 h after NGF treatment.

the cytoplasmic region and neurites, especially in the distal tips and the cylinder of neurites where CRMP-2 and microtubules form the center core (*indicated with white arrows* in Fig. 2, *A–C*). In addition, neurofibromin is particularly expressed in the adhesive membranous site in the neurite distal cone being linked to the core of CRMP-2 and microtubules of PC12 cells. These results demonstrate that neurofibromin and CRMP-2 are co-localized in PC12 cells, especially in the growing neurites during the differentiation of cells, indicating that the interaction of these molecules may influence the regulation of neurite outgrowth in PC12 cells.

The Effects of NF1 siRNA on the Neurite Outgrowth of PC12 Cells after NGF Treatment—To analyze how NF1 functions during neurite outgrowth regulation in association with CRMP-2 after NGF stimulation, knockdown of neurofibromin by NF1 siRNA in PC12 cells was performed, and the phenotypic change of the neurite outgrowth compared with that of the control siRNA transfected cells was then observed. After 48 h following transfection with NF1(249) siRNA or NF1(4383) siRNA, a more than 90% depletion of neurofibromin in PC12 cells was confirmed with Western blotting using anti-NF1 antibody (Fig. 3*A*). Morphological changes of cellular neurite outgrowth after transfection with NF1 siRNAs were precisely analyzed using confocal microscope and time-lapse microscope video analysis. Interestingly, compared with the control cells, which showed normal neurite outgrowth, significant inhibition of neurite outgrowth in PC12 cells was observed after transfection of all types of the NF1 siRNA (Fig. 3, *B* and *C*, supplemental Fig. S1, and supplemental movies 1 and 2). As shown in Fig. 3*B*, *panels a* and *b* (supplemental Fig. S1*A–C*), cells that incorporated fluorescent NF1 siRNA into the peri-nuclear region showed significant inhibition of neurite outgrowth. In contrast, cells that failed to uptake NFI siRNA and cells with NF1 siRNA attached to the cellular surface in a nonspecific manner showed normal neurite outgrowth. This retraction of neurites was detected reproducibly with time-lapse microscope video analysis (Fig. 3*C* and supplemental movies 1 and 2). Especially after 24–48 h of NF1 siRNA transfection, the neurite retraction (collapse) was significantly compared with the control cells in a time-dependent manner (Fig. 3*C*). These results strongly indi-

cate that neurofibromin is required for neurite outgrowth in PC12 cells, and they suggest that the interaction of neurofibromin and CRMP-2 plays an important role in neurite outgrowth in PC12 cells.

Proteomic Differential Analysis between PC12 Cells Treated with NF1 siRNA and Control siRNA by Two-dimensional Fluorescence DIGE—To study the precise differences in protein expression patterns between NF1 siRNA-transfected and control cells, proteomic analysis by two-dimensional fluorescent DIGE was performed. Before analysis, the cell lysates from NF1 siRNA-transfected PC12 cells and control cells were labeled with Cy5-fluora and Cy2-fluora, respectively, and then mixed into one fraction and subjected to two-dimensional PAGE using a 13-cm IPG strip (pI 4–7) for the first dimension, and SDS-PAGE (10%, 13 × 13 cm) for the second dimension of electrophoresis. The two-dimensional images were obtained after scanning with two fluorescent Cy5 and Cy2 filters and analyzed with inferred from direct assay. More than 1,000 protein spots obtained in each scan (control, 1,071 spots; NF1 siRNA, 1,060 spots) were reproducibly detected in each sample (Fig. 4*A*). For over 100 spots, the intensity varied by a factor of more than 1.5 between NF1 siRNA-transfected cells and control cells. Similar results were obtained from another set of two-dimensional DIGE gels for which the Cy2/Cy5 labeling was switched (data not shown).

Among these spots, at least seven differently expressed CRMP-2 proteins were identified in two-dimensional DIGE and two-dimensional Western analysis (Fig. 4, *A–C*). Four major spots for CRMP-2, spots 1–4, appear from right to left (pI 6.0-5.4), and three minor spots, spots 1.5, 2.5, and 3.5, appear between spots 1 and 2, spots 2 and 3, and spots 3 and 4, respectively (Fig. 4*B*, *lower panel*). Interestingly, the intensity of spot 1 was significantly decreased (*red* (siNF1)/*green* (control) = 0.3) after NF1 siRNA transfection (Fig. 4*B*, *upper panel*). For confirmation, the two-dimensional Western pattern of CRMP-2 was semi-quantitatively analyzed using PC12 cell lysates with several conditions. As shown in Fig. 4, *C–E*, the time course analysis after NGF treatment showed that the ratio of spot 1 intensity to total spot intensity was significantly decreased in a time-dependent manner compared with the control cells. We also observed changes in the intensities of the other spots corresponding to CRMP-2 (spots 1.5, 2, 3, and 4) (Fig. 4*C*). In particular, the ratio of spot 1.5 intensity to total spot intensity was increased significantly after NGF stimulation in NF1 siRNA-transfected cells. These results suggested that changes in the spot intensities of CRMP-2 spots may represent changes in the modification status, such as phosphorylations, as well as NF1-related regulation of neurite outgrowth in PC12 cells.

The Effects of NF1-GRD Type I Overexpression in NF1 siRNA-Treated PC12 Cells—To confirm whether the changes in neurite phenotypes and CRMP-2 spot patterns in two dimensions were caused by the suppression of neurofibromin with NF1 siRNA, an expression plasmid corresponding to NF1-GRD type I was transfected to PC12 cells in the presence or absence of NF1 siRNA after NGF treatment. Overexpression of GRD type I, which possesses strong RAS-GAP activity (6), significantly effected to rescue both neurite retraction and CRMP-2 spot shifts, especially the intensities of spot 1 and spot 1.5, which were returned to the control (not treated with NF1 siRNA) levels, in PC12 cells (Fig. 5, *A* and *B*). These results demonstrate that the neurite outgrowth of PC12 cells needs neurofibromin GAP activity and that these phenotypic changes are correlated with the CRMP-2 protein spot shifts.

Analyses of CRMP-2 Phosphorylation Patterns in Two-dimensional DIGE—CRMP-2 has been known as a highly phosphorylated protein in neuronal cells (16). To determine whether each spot corresponding to CRMP-2 was the phosphorylated form or not, we analyzed phosphorylated proteins in PC12 cells by two-dimensional DIGE using phospho-specific protein stainer, ProQuant Diamond. Fig. 6*A* (*lower panel*) shows that ProQuant Diamond staining of spots 1.5, 2, 2.5, 3, 3.5, and 4 was obvious (*yellow* or *orange*), whereas spot 1 was unresponsive to the staining (*green*). This evidence was confirmed with another experiment using Cdk inhibitors that amplify spot 1 with protein (SYPRO Ruby) level but not phosphorylation (ProQuant Diamond) level (supplemental Fig. S2). These results indicated that, among the seven CRMP-2 spots in the two-dimensional gels, only spot 1 represents the nonphosphorylated form, whereas the other spots are phosphorylated forms of CRMP-2. Semi-quantitative analysis of spot intensities by ProQuant staining revealed that specific phosphorylation levels in each protein spot were increased in correlation with decreases in spot pI (Fig. 6*B*). These results suggest that the shift of protein spots from right to left (from pI 5.9 to pI 5.4) reflects the differences in phosphorylation levels of each spot. The specific phosphorylation/protein levels of spots 1.5 and 2 were similar, although the pI of each spot showed a small difference, suggesting that these spots possess the same level of phosphorylation but different phosphorylation sites. Spots 2.5 and 3 also showed similar levels of specific phosphorylation when compared with each other but almost twice the level when compared with the pair of spots 1.5 and 2. This indicated that spots 2.5 and 3 possess different phosphorylation sites and 2 times higher levels of phosphorylation than spots 1.5 and 2.

Identification of the CRMP-2 Phosphorylation Sites in PC12 Cells by Two-dimensional Western Analysis—To identify the phosphorylation sites of CRMP-2 proteins, whose spots were differentially shifted forming a seven-spot pattern (Fig. 7*A*), we analyzed the phosphorylation patterns of CRMP-2 in PC12 cells by Western blotting in several conditions of kinase inhibitors using specific antibodies against phosphorylated CRMP-2. After calyclin A treatment to increase the CRMP-2 phosphorylation levels in PC12 cells (Fig. 7*B*), significant disappearance of CRMP-2 spots 1.5, 2.5, and 3.5 was observed in the presence of the Rho kinase inhibitor (Y27632) (Fig. 7*C*). A specific antibody against the Rho kinase-phosphorylated CRMP-2 (anti-phospho-Thr^{555} CRMP-2 antibody) reacted with those spots (Fig. 7*D*), whereas in the presence of Y2763, these positive spots all disappeared (Fig. 7*E*), suggesting that spot 1.5 could be Thr^{555}-phosphorylated CRMP-2 by Rho kinase and that spots 2.5 and 3.5 could have other phosphorylation sites in addition to Thr^{555}. The specific antibody against GSK-3β-phosphorylated CRMP-2 (anti-phospho-Thr^{514} CRMP-2 antibody) reacted with spots 3 and 4 significantly (Fig. 7*K*). In the presence of GSK-3β inhibitor (LiCl), spots 3 and 4 shifted and displayed

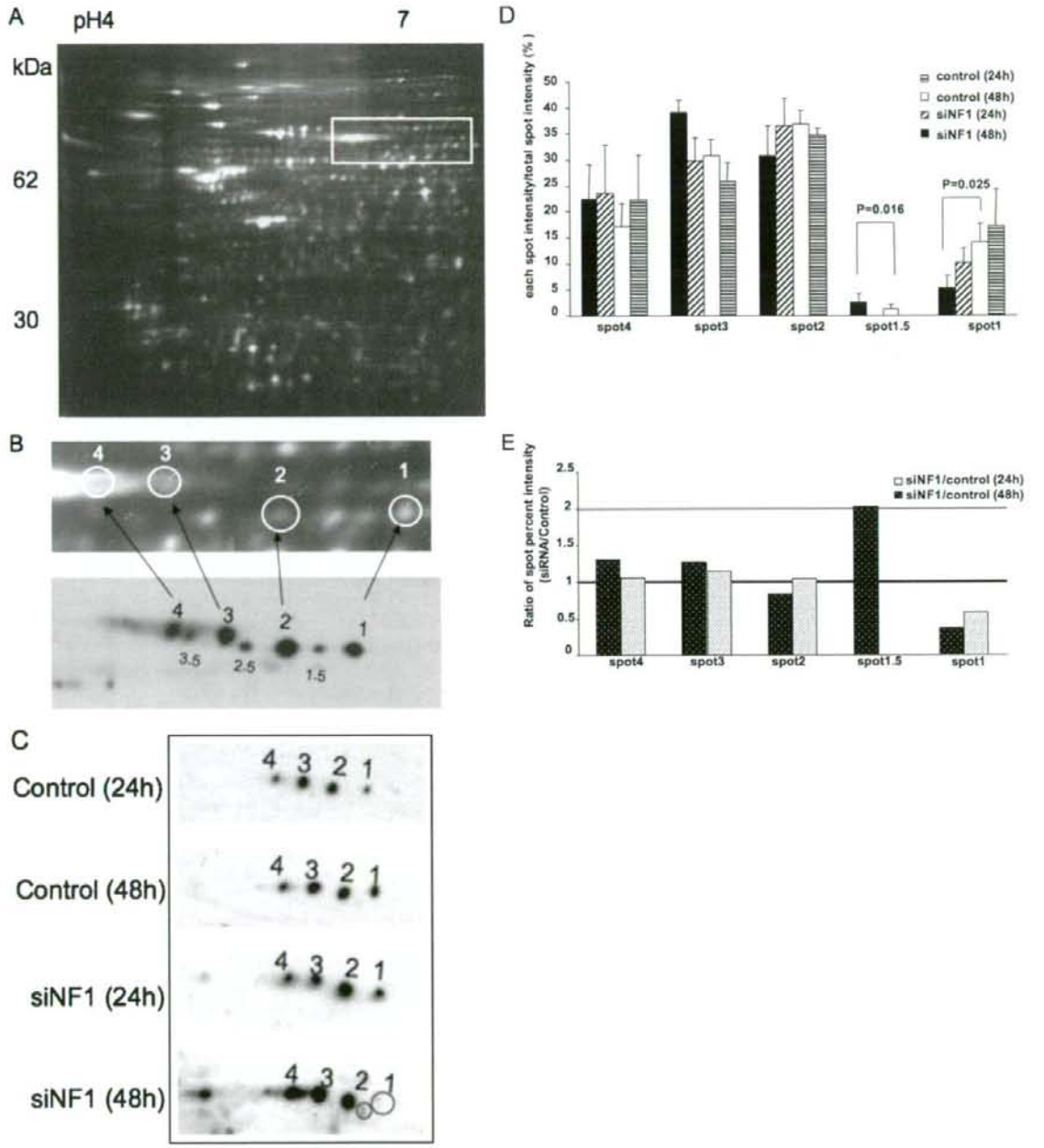

FIGURE 4. **Comparative two-dimensional PAGE analysis of PC12 cells transfected with NF1 siRNA or control siRNA.** *A*, two-dimensional DIGE analysis of PC12 cells transfected with NF1 siRNA (*red*) *versus* control siRNA (*green*). Cellular proteins prepared from PC12 cells transfected with NF1(249) siRNA and control siRNA were labeled with Cy5 (*red*) and Cy2 (*green*), respectively. Two-dimensional patterns (13 × 13 cm) were scanned with Typhoon 9400 and analyzed by Progenesis hands-free analysis. Suppression of NF1 expression by siRNA lead to alteration of the two-dimensional DIGE pattern in PC12 cells. The *inset* indicates the position enlarged in *B*. *B*, identification of CRMP-2 protein spots by two-dimensional Western analysis with anti-CRMP-2 antibodies. *Upper panel* shows two-dimensional DIGE pattern of CRMP-2 enlarged from the *inset* in *A*. *Lower panel* shows CRMP-2 protein spot pattern in two-dimensional Western blotting with anti-CRMP-2 antibodies. Protein spots corresponding to spots 1, 1.5, 2, 2.5, 3, 3.5, and 4 all showed positive against anti-CRMP-2 antibodies. *C–E*, comparison of protein spot intensities of CRMP-2 in PC12 cells transfected with NF1 siRNA *versus* control siRNA. PC12 cells were transfected with NF1(249) siRNA or control siRNA, stimulated with NGF, and harvested after 24 or 48 h of NGF treatment. Each cellular lysate was subjected to two-dimensional Western analysis (7 × 7 cm) using anti-CRMP-2 antibodies (*C*). Percent ratios of each spot intensity in total spot intensity were indicated in each histogram (*D*), and ratios of spot percent intensities of NF1 siRNA *versus* control siRNA of each protein spot 1, 1.5, 2, 3, and 4 in total spot intensity of CRMP-2 were calculated and indicated in each histogram (*E*). The spot intensities of spot 1.5 in both of NF1 siRNA and control cells after 24 h of NGF treatment were below the detection limit. The data were obtained from four separate identical experiments, and these averages, and the significant coefficient of correlation values less than 0.05, are shown in each histogram. *Error bars* represent S.E.

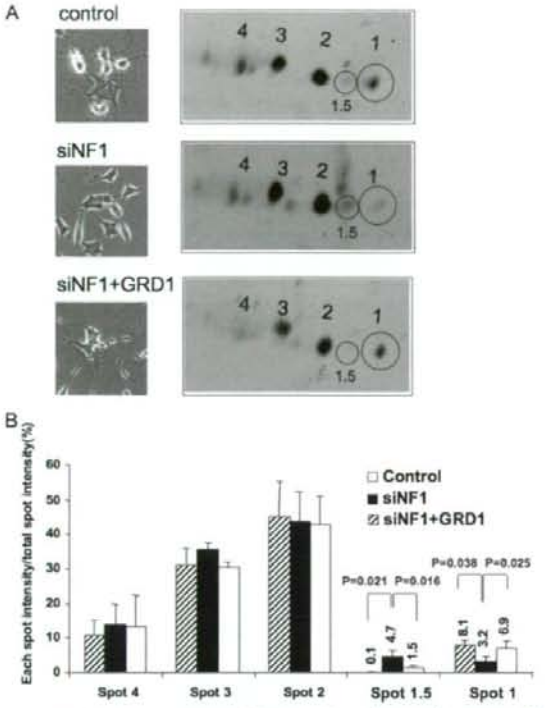

FIGURE 5. **Rescue experiment with NF1-GRD on the neurite outgrowth inhibition and changes of CRMP-2 two-dimensional pattern by NF1-siRNA in PC12 cells.** *A*, control siRNA and NF1(249) siRNA were transfected separately or co-transfected with NF1 (GRD) type 1 into PC12 cells before treating with NGF for 24 h. After 48 h of NGF treatment, cellular morphologies were observed with the phase-contrast microscope (×100) and subjected to the analysis with two-dimensional immunoblotting using anti-CRMP-2 antibody. *B*, comparison of each spot intensity for CRMP-2 after the transfection of NF1 siRNA and NF1 GRD. The *histograms* show the percentage of each spot intensity in total spot intensity of CRMP-2s in individual samples. The intensity of each sample was obtained by two-dimensional Western blotting using anti-CRMP-2 antibody followed by Cy5-labeled secondary antibody. The data were obtained from the average results of the four separate identical experiments, and the significant coefficient of correlation values less than 0.05 are shown in each histogram. *Error bars* represent S.E. of three sets of those experiments.

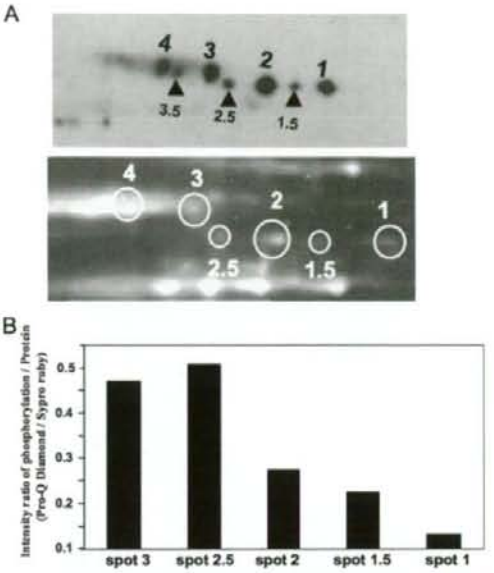

FIGURE 6. **Semi-quantitative two-dimensional PAGE analysis of CRMP-2 phosphorylation using ProQuant Diamond staining.** *A*, phosphorylated CRMP-2s were sequentially shifted to the acidic pI region in two-dimensional gels. Phosphorylated CRMP-2 separated on two-dimensional gels were stained with ProQuant Diamond (*red*) and SYPRO Ruby (*green*), scanned with Typhoon 9400, and merged, respectively. *B*, ratios of each spot intensity stained with ProQuant Diamond for phosphoprotein *versus* SYPRO Ruby for protein. The *y* axis shows the ratio of fluorescent intensities of spots 1, 1.5, 2, 2.5, and 3 obtained from ProQuant Diamond staining *versus* SYPRO Ruby staining. The ratios for spots 3.5 and 4 were not calculated because other unknown protein spots crossed over on those spots and caused difficulties for the calculation.

lower intensities (Fig. 7*L*) or very low reactivity against anti-phospho-Thr^{514} CRMP-2 antibody (Fig. 7*M*), suggesting that spot 3 could possess the phosphorylation site of Thr^{514} by GSK3-β and that spot 4 could possibly have another phosphorylation site such as Thr^{518} or Thr^{509} as reported (17), in addition to Thr^{514}. It is well known that a GSK-3β priming kinase such as Cdk5 is necessary for the GSK-3β phosphorylation of CRMP-2. Thus, we treated the cells with or without a Cdk5 inhibitor, purvalanol A, and the effect on the two-dimensional pattern of CRMP-2 was analyzed. As shown in Fig. 7, *F* and *G*, there were significant decreases in the spot intensities of spots 2–4, and remarkable increases in the intensities of spots 1 and 1.5 in the presence of purvalanol. To confirm these spot shifts were caused by the CDK5 inhibition, the same samples used for Fig. 7, *F* and *G*, were subjected to two-dimensional Western analysis using the specific antibody against Cdk-5-phosphorylated CRMP-2 (anti-phospho-Ser^{522} CRMP-2 antibody). The anti-phospho-Ser^{522} CRMP-2 antibody significantly reacted with spot 2, 2.5, 3, 3.5, and 4 in the absence of the inhibitor (Fig. 7*H*), whereas these reactive spots almost disappeared in the presence of purvalanol (Fig. 7*I*). To confirm our speculation that spot 1 is a real nonphosphorylated form of CRMP-2, the cellular CRMP-2 spot 1 was analyzed by ProQuant Diamond and SYPRO Ruby staining, after Cdk5 inhibitor treatment that significantly amplified the spot 1 intensity in a two-dimensional Western blot (Fig. 7*G*). The intensity of SYPRO Ruby protein staining of spot 1 was increased with Cdk5 inhibitor more than five times, but the intensity of phospho-staining by ProQuant Diamond was not increased compared with those in the control condition, suggesting that spot 1 is a nonphosphorylated CRMP-2 (supplemental Fig. S2). These results strongly indicate that spot 2, which shifted from spot 1, could have a Cdk5 phosphorylation site of Thr^{522} that acts as a priming phosphorylation site for GSK-3β. We also deduced that spots 3 and 4 could both have a phosphorylation site of Thr^{522} in addition to the phosphorylation site of Thr^{514}. The spot 1.5 increased in intensity, whereas spots 2.5 and 3.5 decreased in intensity after purvalanol A treatment suggested that Rho kinase-related spots 2.5 and 3.5 might be involved in the phosphorylation by Cdk5 and/or that the Cdk inhibition caused the Rho kinase activation.

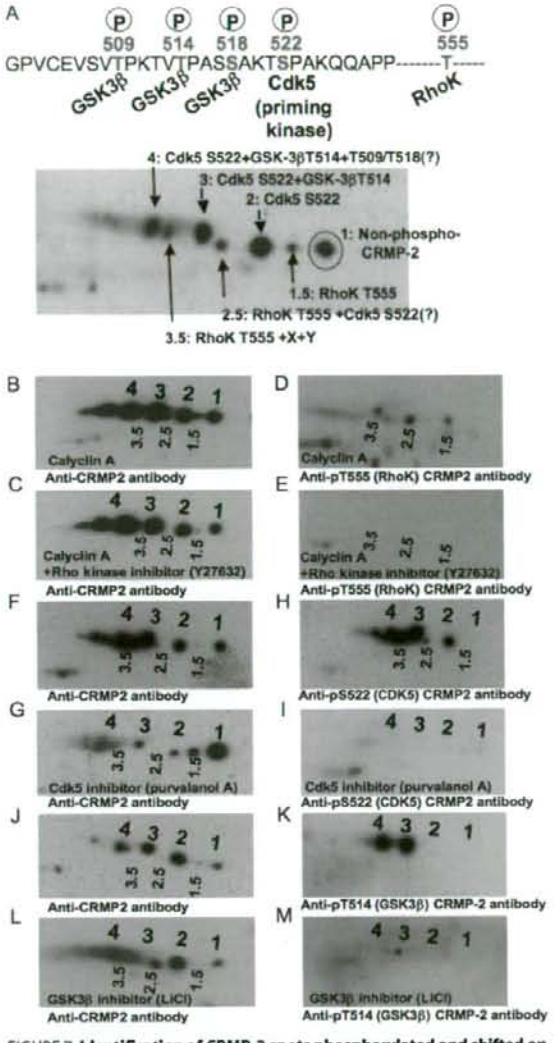

FIGURE 7. **Identification of CRMP-2 spots phosphorylated and shifted on two dimensions by the specific kinases in PC12 cells.** *A*, postulated phosphorylation sites on the amino acid sequence of CRMP-2 (Thr^{509}, Thr^{514}, Ser^{518}, Ser^{522}, and Thr^{555}) and the specific kinases (GSK3β, Cdk5, and Rho kinase) for CRMP-2. *B–E*, identification of CRMP-2 phosphorylated spots by Rho kinase on two dimensions by using Rho kinase inhibitor and anti-phospho-Thr^{555} (Rho kinase) CRMP-2 antibody. After 48 h of NGF treatment, cells were incubated without (*B* and *D*) or with 10 μM Rho kinase inhibitor (Y27632) (*D* and *E*) for 1 h at 37 °C in a CO_2 incubator, and then for 30 min with the addition of calyculin-A (10 μM) in a serum-free condition. After washing, cells were lysed with lysis buffer A and subjected to analysis with two-dimensional immunoblotting using anti-CRMP-2 antibody (*B* and *C*) or anti-phospho-Thr^{555} (Rho kinase) CRMP-2 antibody (*D* and *E*). *F–I*, identification of CRMP-2-phosphorylated spots by Cdk5 on a two-dimensional gel using Cdk5 inhibitor and anti-phospho-Ser^{522} (Cdk5) CRMP-2 antibody. After 48 h of NGF treatment, cells were incubated with (*G* and *I*) or without (*F* and *H*) 10 μM Cdk5 inhibitor (purvalanol A) for 24 h at 37 °C in a CO_2 incubator, and subjected to the analysis with two-dimensional immunoblotting using anti-CRMP-2 antibody (*F* and *G*) or anti-phospho-Ser^{522} (Cdk5) CRMP-2 antibody. *J–M*, identification of CRMP-2-phosphorylated spots by GSK-3β on two dimensions using anti-phospho-Thr^{514} (GSK-3β) CRMP-2 antibody and GSK-3β inhibitor. After 48 h of NGF treatment, cells were incubated with (*L* and *M*) or without (*J* and *K*) GSK-3β inhibitor LiCl (30 mM) for 24 h at 37 °C in a CO_2 incubator, and subjected to analysis with two-dimensional immunoblotting using anti-CRMP-2 antibody (*J* and *L*) or anti-phospho-Thr^{514} (GSK-3β) CRMP-2 antibody (*K* and *M*).

Suppression of Neurofibromin by NF1 siRNA Up-regulated Cdk5, GSK-3β, and RhoK Phosphorylation of CRMP-2 in PC12 Cells after NGF Treatment—It is clearly evident that intensity changes in the protein spots of CRMP-2 caused by kinase inhibitor treatments of PC12 cells reflect the alteration of CRMP-2 phosphorylation status. We speculated that CRMP-2 phosphokinases could be regulated by neurofibromin during neurite outgrowth in PC12 cells. To understand the role of neurofibromin in cellular phosphorylation of CRMP-2 and its significances for neurite outgrowth, we analyzed the effects of kinase inhibitors on CRMP-2 phosphorylation as well as phenotypic changes in PC12 cells after treatment with NF1 siRNA.

PC12 cells stimulated with NGF after suppression of neurofibromin by siRNA were treated with Rho kinase inhibitor (Y27632), and the CRMP-2 two-dimensional Western patterns were analyzed semi-quantitatively. As shown, Fig. 8, *A*, *panel c*, and *B*, *spot 1.5*, designated as a Rho kinase-phosphorylated spot (phospho-Thr^{555}), significantly disappeared. Interestingly, the decrease in spot 1.5 intensity occurred in parallel with a decrease in the intensity of spot 2 (phosphorylated CRMP-2 (phospho-Ser^{522}) by Cdk). In addition, the intensities of spots 3 and 4 (phosphorylated CRMP-2 (phospho-Thr^{514}) by GSK-3β in addition to Cdk5 phosphorylation at phospho-Ser^{522}) were increased in the Rho kinase inhibitor-treated cells combined with NF1-siRNA treatment, compared with the control cells. At the same time, we observed the effect of Rho kinase inhibitor on the neurite retraction caused by NF1-siRNA. RhoK inhibitor showed some effects on the neurite recovery as shown in Fig. 8*A*, *panel c* (*left* and *middle panel*); however, the effects on the extension pattern of neurites and the cellular shape were different (shorter filopodia and a round cell body as shown in Fig. 8*A*, *panel c*) from those of control cells. These results suggest that NF1 siRNA increases the Rho kinase-related phosphorylation of CRMP2 and that combining treatment by Rho kinase inhibitor with NF1 siRNA affects both Rho kinase as well as Cdk5/GSK-3β phosphorylation of CRMP2. These CRMP-2 phosphorylation changes on CRMP-2 may reflect the incomplete neurite recovery in RhoK inhibitor treatment.

On the other hand, the combined treatment of Cdk5 inhibitor (purvalanol A or olomoucine) with NF1 siRNA was significantly effective in decreasing the intensities of spots 2–4 (Fig. 8*A*, *panel d*, and *B*, and supplemental Fig. S3), which were designated as Cdk5 and GSK-3β-related phospho-CRMP-2 respectively. In this condition, the intensity increase of spot 1 (nonphosphorylated CRMP-2) in Cdk5 inhibitor-treated cells was also significant. The intensity of spot 1.5, which is related to Rho kinase, was also increased after Cdk5 inhibitor and NF1 siRNA treatment, suggesting the Cdk5 involvement of spot 1.5 as shown in Fig. 7*G*, Fig. 8, *A*, *panel d*, and *B*, and supplemental Fig. S3, *B* and *C*. These effects dramatically reflected the neurite extension rescuing the retraction by NF1 siRNA as shown in Fig. 8*A*, *panel d*, and supplemental Fig. S3, *B* and *C*, suggesting that NF1 siRNA-related spot 1 intensity decrease and neurite

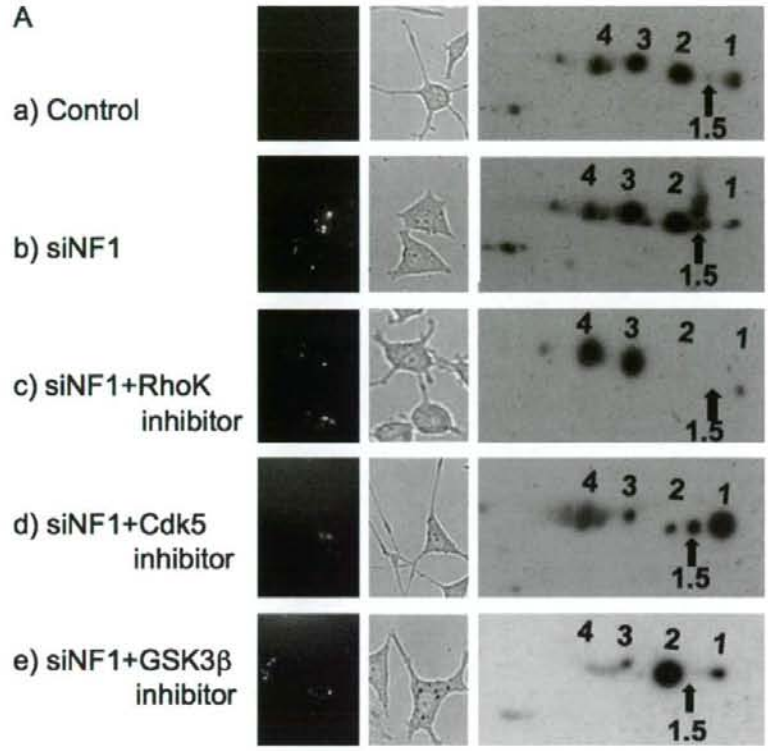

FIGURE 8. **Effects of Rho kinase, Cdk5, and GSK-3β inhibitor on NF1 siRNA-induced CRMP-2 phosphorylation and neuronal retraction in PC12 cells.** *A, right panel,* comparison of the CRMP-2 spot patterns in the NF1 siRNA or control siRNA-treated cells in the presence or absence of Rho kinase, Cdk5, and GSK-3β inhibitors. After 48 h of transfection of NF1 siRNA (*panels b–e*) or control siRNA (*a*) to the NGF-treated PC12 cells, cells were treated with (*panels c–e*) or without (*panels a* and *b*) 10 μM Rho kinase inhibitor (Y27632) (*panel c*), 10 μM Cdk 5 inhibitor (purvalanol A) (*panel d*), or 30 mM GSK-3β inhibitor (LiCl) (*panel e*) and subjected to two-dimensional immunoblotting analysis with anti-CRMP-2 antibody, as described in Fig. 7 and under "Experimental Procedures." *Middle panel,* phase contrast photograph of each cells treated with kinase inhibitors. *Left panel,* fluorescent NF1 siRNA incorporated into the cells. *B,* comparison of each spot intensity for CRMP-2 patterns in the cells that were treated with the same conditions of *A*. The *histograms* show the percentage of each spot intensity per total spot intensity obtained from the average of three separate identical experiments of two-dimensional immunoblotting analysis. *Error bars* represent S.E.

retraction could be mainly caused by Cdk5 activation. In the area of spot 4, which represents more than three phosphorylation sites of CRMP-2, a relatively broad increase in intensity was detected and labeled as Cdk5 inhibitor effects with an unknown reason.

Finally, the effects of combined treatment of GSK-3β inhibitor (LiCl) with NF1 siRNA was analyzed. The result revealed that LiCl treatment was dramatically effective in decreasing the intensities of spots 3 and 4 (Fig. 8, *A, panel e,* and *B*), which were designated as both GSK-3β (phospho-Thr^{514}), and Cdk5 (phospho-Ser^{522})-related phospho-CRMP-2. However, the effect of LiCl on spot 1 was not significant, and its morphological effect of rescuing the neurite retraction was small (Fig. 8*A*, *panel e*). These results demonstrate that individual treatment by the GSK-3β inhibitor stops further sequential phosphorylation of the CRMP-2 spot 2 to spots 3 and 4, but it has little effect functionally on neurite retraction in this system.

From these results, it is indicated that both the NF1 siRNA-related decrease in intensity of spot 1 and the increase in intensity of spot 1.5 are related to the complemental activation of Cdk5, GSK-3β, and the Rho kinase, as well as their phosphorylation of CRMP-2. However, neurofibromin-related neurite regulation, in association with CRMP-2 phosphorylation, may be mainly controlled via the regulation of Cdk5 kinase activity, which strongly controls the intensity of spot 1, the nonphosphorylated active form of CRMP-2.

DISCUSSION

In this study, we demonstrated a novel function of neurofibromin in neurite outgrowth of PC12 cells comprising regulation of CRMP-2 phosphorylation via direct and indirect association with CRMP-2 (supplemental Fig. S5). CRMP-2 was identified as a neurofibromin-binding protein using newly developed proteomic affinity mapping methods. Neurofibromin directly interacts with the active (nonphosphorylated) form of CRMP-2, but not with the inactive (phosphorylated) form of CRMP-2, via the neurofibromin CTD. Immunocytochemical analysis showed that neurofibromin and CRMP2 are co-localized especially in the distal tips and branches along the neurites, which are recognized as major CRMP-2 action sites (18) in differentiated PC12 cells. Depletion of neurofibromin in PC12 cells with NF1

siRNA up-regulated the inactivation of CRMP-2 by phosphorylation, which induced neurite retraction of the cells. The phosphorylation of CRMP-2 is regulated with several kinases, such as Cdk5, GSK-3β, and Rho kinase. Here we present evidence that the phosphorylation of CRMP-2 by these kinases may be regulated by neurofibromin via the direct interaction/complex formation with CRMP-2, and by indirect regulation of these kinase cascades in PC12 cells during neurite outgrowth after NGF treatment.

Previously, we found that time-dependent increases in the GAP activity of cellular neurofibromin (NF1-GAP) were detected after NGF stimulation in PC12 cells, and these increases were correlated with the down-regulation of Ras activity during neurite elongation (6). Interestingly, when cellular NF1-GAP activity was inhibited with dominant-negative (DN) forms of NF1-GRD type I, neurite extension of PC12 cells was significantly inhibited. This correlated with prolonged Ras activation and longer stimulation by NGF (6).

Similar results were obtained in the present study using NF1 siRNA, which caused depletion of neurofibromin and significant inhibition of neurite outgrowth. Forty eight hours of observation with a time-lapse microscope directly following NGF addition showed that PC12 cells transfected with NF1 siRNA displayed weak and short neurite extension, which quickly resulted in retraction (Fig. 3 and supplemental movies 1 and 2). Phenotypic changes were also observed in the rat embryonic hippocampal primary neuron whose axonal extension was significantly reduced after treatment with NF1 siRNA,[3] as we observed a similar result in previous studies with using GRD-DN overexpression (6). The rescue experiment performed by overexpressing the high NF1-GAP activity FLAG-GRD type I (6) was successful in both changing neurite outgrowth and the CRMP-2 phosphorylation pattern (Fig. 5, *A* and *B*). Thus, it could be concluded that cellular Ras regulation by NF1-GAP is one of the most important events in neuronal development, although another function of neurofibromin in addition to NF1-GAP activity may also be part of this mechanism.

Most of the *NF1* mutations are nonsense, frameshift, or truncating mutations leading to premature termination codons (19, 20), and a relatively high frequency of the mutations have been reported downstream of the GRD in the C-terminal region. This suggested that the neurofibromin C terminus is a crucial region in regulating neurofibromin function. In our previous study, we identified several functional proteins, such as 14-3-3s (14) and DDAH (10), that bound to the C-terminal NF1 and affected the GAP activity of neurofibromin, suggesting that the C-terminal region of neurofibromin could be a regulatory domain for GRD activity. In this context, identification and analysis of cellular proteins that are bound to C-terminal neurofibromin are thought to be crucial to elucidate the biological significance of neurofibromin.

In this study, at least 58 proteins associating with neurofibromin (Table 1) were identified semi-quantitatively with (iTRAQ) using micro-affinity columns and NanoLC ESI/MALDI-MS/MS analysis. These proteins contained several neuronal regulating proteins, including not only previously known but also novel proteins, such as CRMP-2, which is known as an axon regulatory cargo protein. This information moved us to analyze the mutual association of CRMP-2 and neurofibromin in conjunction with neuronal function.

Collapsin-response mediator proteins are a family of cytosolic proteins developmentally regulated in the nervous system (21–24), which are assumed to mediate intracellular responses to collapsin (25). Collapsin-response mediator proteins have significant homology with the product of *unc*-33 in *Caenorhabditis elegans*, the mutation of which results in abnormal axon outgrowth (26–28). CRMP-2 directly binds to kinesin light chain (KLC1) and tubulin, resulting in a trimeric complex that regulates tubulin transport to the distal part of the growing axon (29). Analogous to the CRMP-2-tubulin interaction, it is speculated that neurofibromin could be a new CRMP-2-related cargo or complex protein that functions as a regulator of the axon formation complex. It was reported that interaction between CRMP-2 and tubulin was altered by CRMP-2 phosphorylation by Cdk5, GSK-3β (30), and by Rho kinase (11). In our study, the interactions of neurofibromin, CRMP-2, and tubulin were confirmed with immunoprecipitation assay using each of their respective antibodies, and it was found that neurofibromin and tubulin could bind strongly to the nonphosphorylated form of CRMP-2, as we expected (Fig. 1, *C* and *D*).

In general, the phosphorylation of CRMP-2 has been analyzed using one-dimensional Western blotting, after which it has been assessed whether the band for CRMP-2 shifts up or not. Our strategies used in this study, such as two-dimensional DIGE combined with a specific staining for phosphorylated proteins (ProQuant Diamond) and two-dimensional Western blotting using specific antibodies, could be an original method to identify a series of CRMP-2 protein spots with varying types of phosphorylation. We identified the specific phosphorylation sites of CRMP-2 by Rho kinase, Cdk5, and GSK-3β in PC12 cells and demonstrated that the neurite retraction is exacerbated by the combinatorial up-regulation of CRMP-2 phosphorylation. As we summarized in Figs. 7 and 8, CRMP-2 phosphorylation is represented starting with a shift in intensity from spot 1 to spot 2 caused by the up-regulation of Cdk5. Spot 2 contains the first phosphorylation site by Cdk5 (Ser^{522}), followed by GSK-3β activation adding the second phosphorylation (Thr^{514}) on spot 3, and the third phosphorylation (possibly Thr^{518}, Thr^{509}, or another) on spot 4. In a parallel manner, spot 1.5, corresponding to Rho kinase-related phospho-CRMP-2 (Thr^{555}), is revealed and followed by the other two phosphorylations on spots 2.5 and 3.5. It is reasonable to speculate that the regulation of neurofibromin-related Ras signaling is necessary for CRMP-2 phosphorylation and neurite outgrowth, because these changes in the spot intensities were rescued with the overexpression of NF1-GRD (6) (Fig. 5).

When we focus on the intensity alteration of spot 1, an active form of CRMP-2 (nonphosphorylated form), a part of the mechanism of neurofibromin-dependent neurite regulation could be simply interpreted in association with CRMP-2 function. First, this active CRMP-2 can form a complex with neurofibromin to maintain the activity to process the neurite outgrowth with NGF treatment, where NF1-GAP may contribute to slow the Ras signal cascade related to CRMP-2 phosphorylation such as MAPK-Cdk5-GSK-3β, Rho-RhoK, and others. Second, neurofibromin depletion by siRNA treatment signifi-

[3] N. Araki, S. Patrakitkomjorn, N. Arimura, and K. Kaibuchi, unpublished observations.

cantly decreased spot 1 intensity and increased the Cdk5, GSK-3β RhoK-dependent phosphorylation on CRMP-2, and this was correlated with the neurite retraction of PC12 cells. Third, the decrease of the CRMP-2 spot 1 and the neurite retraction were significantly rescued with NF1-GAP domain overexpression (Fig. 5) or Cdk5 inhibitor treatment (Fig 8*A, panel d*, and supplemental Fig. S3). Thus, we speculate that the increase of nonphosphorylated CRMP-2 (spot 1) is most important for the neurite outgrowth, and that this was regulated with neurofibromin by inhibiting both Cdk5 activity and CRMP-2 phosphorylation (supplemental Fig. S5).

Concerning spots 2–4, the ratio of their combined spot intensity (CSI) to the total spot intensity (TSI) (spots 1–4) was significantly increased after NF1 siRNA treatment because spot 1 decreased in a statistically significant manner, suggesting that the activation of Cdk5 and that of GSK-3β thereafter may be controlled by neurofibromin depletion. Inhibition of neurite outgrowth was correlated with the increases in the CSI ratio, and phenotypic changes were rescued by NF1-GAP domain overexpression or Cdk5 inhibitor treatment. Nevertheless, only a partial effect was observed with the GSK-3β inhibitor, which magnified the significant increase of spot 2 and the decrease of spots 3 and 4 (Fig. 8), suggesting that the main factor of the NF1-related regulation of neurite outgrowth and CRMP-2 phosphorylation may be Cdk5, but also GSK-3β may function as a player working with its priming kinase Cdk5 to accelerate the phosphorylation of CRMP2 and cause the decrease of the active form of CRMP-2 (spot 1), thereby relating indirectly to the neurite regulation in this system.

On the other hand, spot 1.5 (RhoK-phosphorylated CRMP-2 (phospho-Thr^{555}) was significantly increased after NF1 siRNA treatment, suggesting that the activation of RhoK is controlled by the neurofibromin depletion. Inhibition of neurite outgrowth was also correlated with the increase in spot 1.5 intensity, and these phenotypic changes were rescued by NF1-GAP domain overexpression or RhoK inhibitor (although the effect of RhoK inhibitor for neurite recovery was partial) as shown in Figs. 5 and 8. This suggested that the activation of RhoK was at least controlled by the neurofibromin depletion, and some part of the NF1-related regulation of neurite outgrowth and CRMP-2 phosphorylation could involve RhoK regulation.

After Cdk5 inhibitor treatment, the increase in spot 1.5 by NF1 depletion was more significant and reproducible (Fig. 8). This was speculated that increase of spot 1.5 is partly caused by the shift and decrease of spots 2.5 and 3.5 after Cdk 5 inhibitor treatment. Because they have Cdk phosphorylation site in addition to the Rho kinase site, their shift to the spot 1.5 position by the inhibition of Cdk5 resulted in the increase of the intensity of spot 1.5. Spots 2.5 and 3.5 were also increased after NF1 depletion and rescue experiments with NF1-GAP domain overexpression or RhoK inhibitor looked effective in decreasing those spot intensities, although these spots were originally too small to calculate statistically. Thus, in this study we do not discuss in depth the intensity changes of 2.5 and 3.5 spots, and their relation to the neurite outgrowth. The NF1-GAP-related regulatory signals in neuronal cells such as Ras-MAPK, Ras-PI3K (6), and Rho-RhoK/ROCK-LIMK (9) have been reported previously. In this study, we are the first to demonstrate that the phosphorylations of CRMP-2 by Cdk5, GSK-3β, and Rho/Rho kinase, which are regulated with neurofibromin, play a role in the neurite outgrowth of PC12 cells (supplemental Fig. S5).

Concerning the functional association of Rho/Rho kinase to cellular neurofibromin, in our previous study we demonstrated that neurofibromin depletion by NF1 siRNA activates cell motility by regulating the dynamics and reorganization of actin filaments via the Rho-RhoK/ROCK-LIMK2-cofilin pathway (9). Recently, several lines of evidence have also implicated the Rho kinase/ROCK-LIMK-cofilin pathway in the regulation of axon growth and guidance in neuronal cells (31–35). Although CRMP-2 phosphorylation by Rho kinase has been reported during the lysophosphatidic acid-induced growth cone collapse in neurons, this could be the first study to implicate the Rho-Rho kinase pathway as causing neurite retraction in PC12 cells after neurofibromin (NF1-GAP) depletion.

Cdk5 is also reported as being activated mainly in post-mitotic cells such as neurons (36) and is suggested to play important roles in neurite outgrowth (37) and neuron migration (38). Cdk5 also modulates protein kinase reactions such as Rac-dependent phosphorylation of p21, which results in modification of the actin cytoskeleton (39). Because the Ras-MAPK signal transcriptionally up-regulates p35 protein, which is an active binding unit for Cdk5, our demonstration of the up-regulation of Cdk5 via NF1-GAP depletion and Ras activation seems reasonable (supplemental Fig. S5).

On GSK-3β function, the report showing that Ras-PI3K-AKT signal activation causes the inactivation of GSK-3β and enhances neurite outgrowth rates in PC12 cells (40–42) looked controversial, considering our results showed that Ras signal activation caused by NF1-GAP depletion resulted in GSK-3β activation, up-regulation of CRMP-2 phosphorylation, and neurite retraction. However, there are several reports strongly demonstrating that GSK-3β is activated via the activation of Cdk5 as a priming kinase (17), and also via Rho-related signal activation (31), supporting our speculation that activation of Cdk5 and Rho/RhoK after neurofibromin depletion can affect the up-regulation of GSK-3β (supplemental Fig. S2).

The direct evidence on the relationship between neurofibromin binding to CRMP-2 and neuronal differentiation could be important to understand the mechanism of this study more correctly. To obtain the information related to this, NF1-CTD was overexpressed in PC12 cells to inhibit the cellular binding of neurofibromin to CRMP-2. After NGF stimulation of PC12 cells, the GFP-NF1-CTD fluorescence was detected successfully in the cells, and their neurite outgrowth was significantly inhibited compared with that of GFP-Mock cells as shown in supplemental Fig. S4. However, in addition to this cellular event, we noticed that the effect of the CTD overexpression on the neurite outgrowth was morphologically different from that in the NF1 siRNA-treated cells. For instance, the GFP-CTD-transfected cells represented a smaller size of the cellular body than those of control cells, and cell detachment was frequently observed. We speculate that the NF1-CTD may work as a regulatory domain for other binding partners, such as tubulins, actin, cofilin, Arp2/3 complex cytoskeletal-organizing proteins, and so on (as shown in Table 1), to collaborate and obtain another cellular function in PC12 cells. Thus, we conclude that

NF1-CTD overexpression could not be a simple "decoy" for the cellular binding of CRMP-2 and neurofibromin but that it could have a more complex function existing in this system to be clarified. Further study will be needed to understand this mechanism underlying neurofibromin functions associated with other binding partners in the neuronal cellular differentiation.

In conclusion, we postulate a novel function of cellular neurofibromin associated with CRMP-2 activity in which it performs two complementary roles (supplemental Fig. S5). First, neurofibromin directly regulates CRMP-2 activation through association, which may protect the phosphorylation sites or change the conformation of CRMP-2 and, in turn, prevent the exposure of CRMP-2 to several kinases such as Rho kinase, Cdk5, and GSK-3β. By the suppression of neurofibromin, the chance of CRMP-2 being exposed to its kinases could be increased. Second, neurofibromin indirectly regulates CRMP-2 by suppressing CRMP-2-phosphorylating kinases. Neurofibromin activity (NF1-GAP) may regulate CRMP-2 phosphokinase activities via the regulation of Ras-related signal pathways, such as MAPK-Cdk5- GSK-3β and Rho-Rho kinase. The suppression of neurofibromin can result in the inhibition of neurite outgrowth via increased activity of Ras signals, which activates kinases involved in CRMP-2 phosphorylation. By using NGF-stimulated PC12 cells as a model, our study has demonstrated a possible cellular function of neurofibromin in neuronal cell differentiation. Further studies based on our findings will shed light on the mechanism of NF1-related neuronal pathogenesis, such as learning disability and memory retardation.

Acknowledgments—We thank Prof. Yoshio Goshima (Department of Molecular Pharmacology and Neurobiology, Yokohama City University Graduate School of Medicine) for providing us anti-phosphorylated CRMP2 (pS522) antibody. We also thank the entire staff of the Tumor Genetics and Biology Department at Kumamoto University for helpful discussion, especially M. Hayashida, K. Cho, M. Junking, A. Silsirivanit, and M. Nagayama for collaborative endeavors; Y. Fukushima, M. Morikawa, and M. Shimono for secretarial assistance; and A. Wilson for manuscript editing. We are also grateful to staff members of the Proteomic Analysis Core System on General Research Core Laboratory, Kumamoto University Medical School, for important contributions to the experiments.

REFERENCES

1. Stephens, K., Riccardi, V. M., Rising, M., Ng, S., Green, P., Collins, F. S., Rediker, K. S., Powers, J. A., Parker, C., and Donis-Keller, H. (1987) *Genomics* **1,** 353–357
2. Cawthon, R. M., Weiss, R., Xu, G. F., Viskochil, D., Culver, M., Stevens, J., Robertson, M., Dunn, D., Gesteland, R., O'Connell, P., and White, R. (1990) *Cell* **62,** 193–201
3. Costa, R. M., Federov, N. B., Kogan, J. H., Murphy, G. G., Stern, J., Ohno, M., Kucherlapati, R., Jacks, T., and Silva, A. J. (2002) *Nature* **415,** 526–530
4. Guo, H. F., Tong, J., Hannan, F., Luo, L., and Zhong, Y. (2000) *Nature* **403,** 895–898
5. Gregory, P. E., Gutmann, D. H., Mitchell, A., Park, S., Boguski, M., Jacks, T., Wood, D. L., Jove, R., and Collins, F. S. (1993) *Somatic Cell Mol. Genet.* **19,** 265–274
6. Yunoue, S., Tokuo, H., Fukunaga, K., Feng, L., Ozawa, T., Nishi, T., Kikuchi, A., Hattori, S., Kuratsu, J., Saya, H., and Araki, N. (2003) *J. Biol. Chem.* **278,** 26958–26969
7. Xu, H., and Gutmann, D. H. (1997) *Brain Res.* **759,** 149–152
8. Li, C., Cheng, Y., Gutmann, D. A., and Mangoura, D. (2001) *Brain Res. Dev. Brain Res.* **130,** 231–248
9. Ozawa, T., Araki, N., Yunoue, S., Tokuo, H., Feng, L., Patrakitkomjorn, S., Hara, T., Ichikawa, Y., Matsumoto, K., Fujii, K., and Saya, H. (2005) *J. Biol. Chem.* **280,** 39524–39533
10. Tokuo, H., Yunoue, S., Feng, L., Kimoto, M., Tsuji, H., Ono, T., Saya, H., and Araki, N. (2001) *FEBS Lett.* **494,** 48–53
11. Fukata, Y., Itoh, T. J., Kimura, T., Menager, C., Nishimura, T., Shiromizu, T., Watanabe, H., Inagaki, N., Iwamatsu, A., Hotani, H., and Kaibuchi, K. (2002) *Nat. Cell Biol.* **4,** 583–591
12. Yoshimura, T., Kawano, Y., Arimura, N., Kawabata, S., Kikuchi, K., and Kaibuchi, K. (2005) *Cell* **120,** 137–149
13. Bollag, G., McCormick, F., and Clark, R. (1993) *EMBO J.* **12,** 1923–1927
14. Feng, L., Yunoue, S., Tokuo, H., Ozawa, T., Zhang, D., Patrakitkomjorn, S., Ichimura, T., Saya, H., and Araki, N. (2004) *FEBS Lett.* **557,** 275–282
15. Byk, T., Dobransky, T., Cifuentes-Diaz, C., and Sobel, A. (1996) *J. Neurosci.* **16,** 688–701
16. Byk, T., Ozon, S., and Sobel, A. (1998) *Eur. J. Biochem.* **254,** 14–24
17. Cole, A. R., Causeret, F., Yadirgi, G., Hastie, C. J., McLauchlan, H., McManus, E. J., Hernandez, F., Eickholt, B. J., Nikolic, M., and Sutherland, C. (2006) *J. Biol. Chem.* **281,** 16591–16598
18. Lee, S., Kim, J. H., Lee, C. S., Kim, Y., Heo, K., Ihara, Y., Goshima, Y., Suh, P. G., and Ryu, S. H. (2002) *J. Biol. Chem.* **277,** 6542–6549
19. Dasgupta, B., and Gutmann, D. H. (2003) *Curr. Opin. Genet. Dev.* **13,** 20–27
20. Fahsold, R., Hoffmeyer, S., Mischung, C., Gille, C., Ehlers, C., Kucukceylan, N., Abdel-Nour, M., Gewies, A., Peters, H., Kaufmann, D., Buske, A., Tinschert, S., and Nurnberg, P. (2000) *Am. J. Hum. Genet.* **66,** 790–818
21. Minturn, J. E., Geschwind, D. H., Fryer, H. J., and Hockfield, S. (1995) *J. Comp. Neurol.* **355,** 369–379
22. Hamajima, N., Matsuda, K., Sakata, S., Tamaki, N., Sasaki, M., and Nonaka, M. (1996) *Gene (Amst.)* **180,** 157–163
23. Ozon, S., Byk, T., and Sobel, A. (1998) *J. Neurochem.* **70,** 2386–2396
24. Wang, L. H., and Strittmatter, S. M. (1996) *J. Neurosci.* **16,** 6197–6207
25. Goshima, Y., Nakamura, F., Strittmatter, P., and Strittmatter, S. M. (1995) *Nature* **376,** 509–514
26. Hedgecock, E. M., Culotti, J. G., Thomson, J. N., and Perkins, L. A. (1985) *Dev. Biol.* **111,** 158–170
27. Hedgecock, E. M., Culotti, J. G., Hall, D. H., and Stern, B. D. (1987) *Development (Camb.)* **100,** 365–382
28. Desai, C., Garriga, G., McIntire, S. L., and Horvitz, H. R. (1988) *Nature* **336,** 638–646
29. Kimura, T., Watanabe, H., Iwamatsu, A., and Kaibuchi, K. (2005) *J. Neurochem.* **93,** 1371–1382
30. Uchida, Y., Ohshima, T., Sasaki, Y., Suzuki, H., Yanai, S., Yamashita, N., Nakamura, F., Takei, K., Ihara, Y., Mikoshiba, K., Kolattukudy, P., Honnorat, J., and Goshima, Y. (2005) *Genes Cells* **10,** 165–179
31. Sayas, C. L., Moreno-Flores, M. T., Avila, J., and Wandosell, F. (1999) *J. Biol. Chem.* **274,** 37046–37052
32. Luo, L. (2000) *Nat. Rev. Neurosci.* **1,** 173–180
33. Hirose, M., Ishizaki, T., Watanabe, N., Uehata, M., Kranenburg, O., Moolenaar, W. H., Matsumura, F., Maekawa, M., Bito, H., and Narumiya, S. (1998) *J. Cell Biol.* **141,** 1625–1636
34. Bito, H., Furuyashiki, T., Ishihara, H., Shibasaki, Y., Ohashi, K., Mizuno, K., Maekawa, M., Ishizaki, T., and Narumiya, S. (2000) *Neuron* **26,** 431–441
35. Nakayama, A. Y., Harms, M. B., and Luo, L. (2000) *J. Neurosci.* **20,** 5329–5338
36. Lew, J., Huang, Q. Q., Qi, Z., Winkfein, R. J., Aebersold, R., Hunt, T., and Wang, J. H. (1994) *Nature* **371,** 423–426
37. Nikolic, M., Dudek, H., Kwon, Y. T., Ramos, Y. F., and Tsai, L. H. (1996) *Genes Dev.* **10,** 816–825
38. Chae, T., Kwon, Y. T., Bronson, R., Dikkes, P., Li, E., and Tsai, L. H. (1997) *Neuron* **18,** 29–42
39. Nikolic, M., Chou, M. M., Lu, W., Mayer, B. J., and Tsai, L. H. (1998) *Nature* **395,** 194–198
40. Owen, R., and Gordon-Weeks, P. R. (2003) *Mol. Cell. Neurosci.* **23,** 626–637
41. Cole, A., Frame, S., and Cohen, P. (2004) *Biochem. J.* **377,** 249–255
42. Yoshimura, T., Arimura, N., Kawano, Y., Kawabata, S., Wang, S., and Kaibuchi, K. (2006) *Biochem. Biophys. Res. Commun.* **340,** 62–68

Mass spectrometric analysis of microtubule co-sedimented proteins from rat brain

Tatsuhiko Sakamoto[1,2], Akiyoshi Uezu[1], Shinya Kawauchi[1], Takuya Kuramoto[1], Koji Makino[1], Kazuaki Umeda[1], Norie Araki[3], Hideo Baba[2] and Hiroyuki Nakanishi[1,*]

[1]*Department of Molecular Pharmacology, and*
[2]*Department of Gastroenterological Surgery, and*
[3]*Department of Tumor Genetics and Biology, Graduate School of Medical Sciences, Kumamoto University, Kumamoto 860-8556, 1-1-1 Honjo, Kumamoto 860-8556, Japan*

Microtubules (MTs) play crucial roles in a variety of cell functions, such as mitosis, vesicle transport and cell motility. MTs also compose specialized structures, such as centrosomes, spindles and cilia. However, molecular mechanisms of these MT-based functions and structures are not fully understood. Here, we analyzed MT co-sedimented proteins from rat brain by tandem mass spectrometry (MS) upon ion exchange column chromatography. We identified a total of 391 proteins. These proteins were grouped into 12 categories: 57 MT cytoskeletal proteins, including MT-associated proteins (MAPs) and motor proteins; 66 other cytoskeletal proteins; 4 centrosomal proteins; 10 chaperons; 5 Golgi proteins; 7 mitochondrial proteins; 62 nucleic acid-binding proteins; 14 nuclear proteins; 13 ribosomal proteins; 28 vesicle transport proteins; 83 proteins with diverse function and/or localization; and 42 uncharacterized proteins. Of these uncharacterized proteins, six proteins were expressed in cultured cells, resulting in the identification of three novel components of centrosomes and cilia. Our present method is not specific for MAPs, but is useful for identifying low abundant novel MAPs and components of MT-based structures. Our analysis provides an extensive list of potential candidates for future study of the molecular mechanisms of MT-based functions and structures.

Introduction

Microtubules (MTs) play crucial roles in a variety of functions within cells, such as mitosis, vesicle and organelle transport, cell motility and morphology, and maintenance of cell polarity (Kirschner & Mitchison 1986; Rogers & Gelfand 2000; Cassimeris & Spittel 2001; Rodriguez *et al.* 2003; Siegrist & Doe 2007). MTs also compose specialized structures, including centrosomes, spindles, basal bodies, cilia and flagella (Wemmer & Marshall 2004; Bettencourt-Dias & Glover 2007; Linck & Stephens 2007; Satir & Christensen 2007). The ability of MTs to participate in these different functions and structures is assumed to be due to a variety of MT-associated proteins (MAPs) and motor proteins. In this study, MAPs are defined as non-motor proteins that directly associate with MTs. To understand the molecular mechanisms of MT-based functions and structures, it is important to identify and characterize MAPs.

Several approaches have been developed to identify MAPs. These include biochemical purification methods (Vallee *et al.* 1984; Olmstead 1986; Cassimeris & Spittel 2001). One biochemical purification approach involves the polymerization of endogenous tubulin in the presence of an MT-stabilizing agent, taxol, followed by co-sedimentation of MTs and their bound proteins. This procedure is often followed by cycles of polymerization and depolymerization to enrich the MAPs. MAP2 and τ were originally identified from brain tissues by this MT co-sedimentation method (Vallee *et al.* 1984; Olmstead 1986; Cassimeris & Spittel 2001). The addition of exogenous MTs has been used as an alternative method to facilitate the recovery of MAPs (Richard & Kreis 1990). Most MAPs that have been identified by this MT co-sedimentation method are relatively abundant proteins that bind along the entire length of MTs.

Communicated by: Yoshimi Takai
**Correspondence*: Email: hnakanis@gpo.kumamoto-u.ac.jp

DOI: 10.1111/j.1365-2443.2008.01175.x

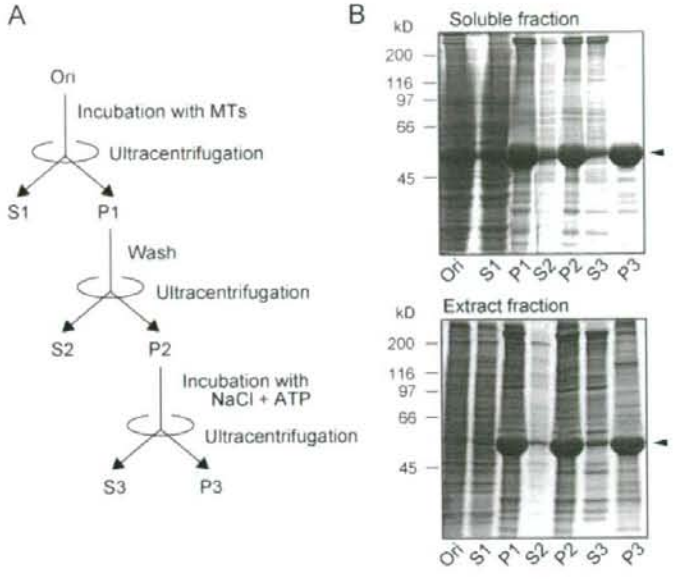

Figure 1 Preparation of MT co-sedimented proteins. (A) Flow diagram. (B) Protein-stained gel. The soluble and extract fractions of rat brain were incubated with MTs, followed by ultracentrifugation. The resultant supernatant and pellet fractions were designated as S1 and P1, respectively. P1 was homogenized and then subjected to ultracentrifugation. The supernatant and pellet fraction were designated as S2 and P2, respectively. P2 was treated with NaCl and ATP to dissociate co-sedimented proteins from MTs, followed by ultracentrifugation. The resultant supernatant and pellet fraction were designated as S3 and P3, respectively. An aliquot of each fraction was subjected to SDS-PAGE (10% polyacrylamide gel), followed by protein staining with Coomassie Brilliant Blue. Ori, original sample; arrowheads, tubulin.

None of the MAPs identified by this method has been found to be localized at MT-based structures, such as centrosomes and cilia. This may be due to the low abundance of components of these MT-based structures. These low abundant proteins may not easily be detected by conventional MT co-sedimentation methods. To enrich and detect low abundant MAPs, MT affinity column chromatography was developed (Kellogg *et al.* 1989). This chromatography method identified components of centrosomes, spindles and kinetochores, although it was not determined whether they were true MAPs.

The recent development of mass spectrometry (MS) allowed several groups to analyze components of isolated MT-based structures, such as centrosomes, cilia and mitotic spindles (Ostrowski *et al.* 2002; Andersen *et al.* 2003; Keller *et al.* 2005; Pazour *et al.* 2005; Sauer *et al.* 2005; Nousiainen *et al.* 2006; Reinders *et al.* 2006). In this study, we prepared MT co-sedimented proteins; exogenous MTs were added to the soluble and extract fractions from rat brain, followed by co-sedimentation of MTs and their bound proteins. MT co-sedimented proteins were then subjected to BioAssist Q anion exchange column chromatography to enrich and detect low abundant proteins, followed by tandem MS (MS/MS) analysis. We identified low abundant MAPs and novel components of centrosomes and cilia.

Results

Preparation and resolution of MT co-sedimented proteins

Rat brains were homogenized in the presence of Triton X-100, followed by ultracentrifugation. The supernatant and pellet fractions were employed as the soluble and insoluble fractions, respectively. From the insoluble fraction, proteins were extracted with a high concentration of NaCl, and the extract was diluted to reduce the concentration of NaCl and used as the extract fraction. When the soluble and extract fractions were incubated with MTs, followed by ultracentrifugation, bound proteins were recovered with MTs in the pellet (P1) (Fig. 1A and B). After the pellet was washed, the resultant pellet (P2) was treated with a high concentration of NaCl and ATP to release the bound proteins from MTs. The released proteins (S3) were collected as MT co-sedimented proteins and subjected to BioAssist Q column chromatography to enrich and detect low abundant proteins. Each fraction was then resolved by polyacrylamide gel electrophoresis (PAGE) (Fig. 2). After staining, each protein band was excised and then in-gel digested with trypsin. Extracted peptides were identified by MS/MS. The sequences obtained were subjected to a search for sequence similarity against

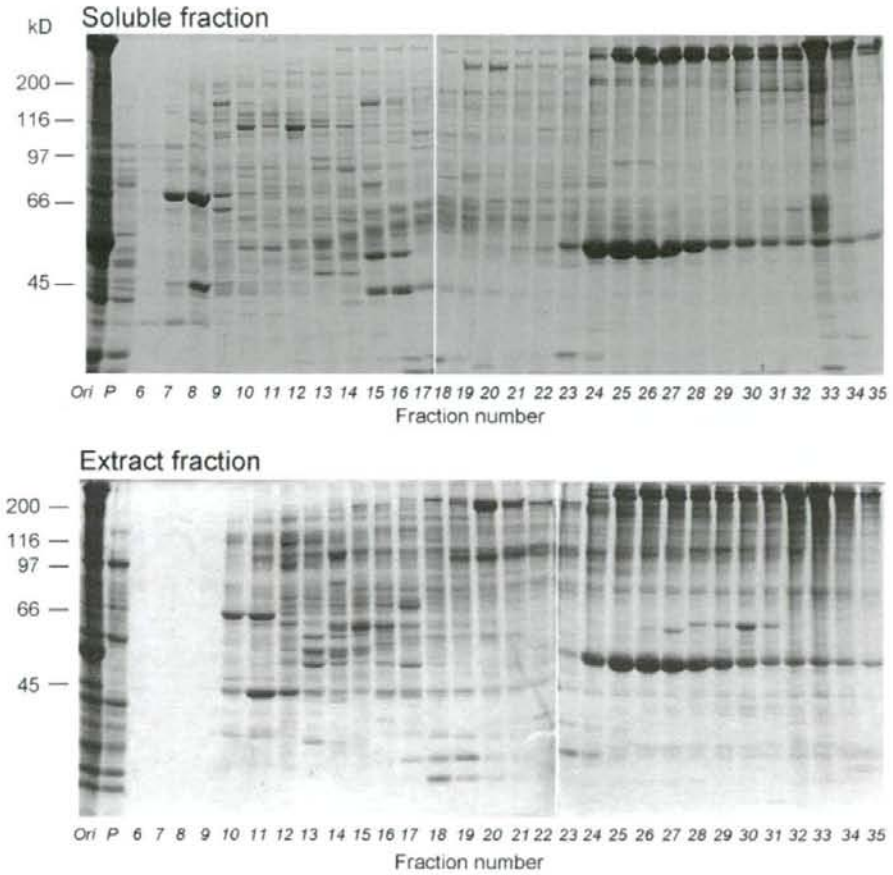

Figure 2 BioAssist Q column chromatography. MT co-sedimented proteins from the soluble and extract fractions were subjected to BioAssist Q column chromatography. An aliquot of each fraction was subjected to SDS-PAGE (10% polyacrylamide gel), followed by protein staining with Coomassie Brilliant Blue. Ori, original sample; P, pass-through fraction.

the non-redundant Swiss-Prot database. As an example for the quality of MS/MS, Fig. 3 shows a fragmentation spectrum of one peptide derived from EB3, an MAP. This spectrum showed excellent signal : noise ratio and good coverage of the expected fragment mass.

Identification of MT co-sedimented proteins

A total of 1237 protein bands (soluble fraction, 505 bands and extract fraction, 732 bands) were excised and subjected to MS/MS analysis. Database searches resulted in the identification of a total of 391 different proteins (soluble fraction, 235 proteins and extract fraction, 222 proteins) (Table 1). The proteins identified were grouped into 12 different categories on the basis of functions and/or localization: 57 MT cytoskeletal proteins, including MAPs and motor proteins; 66 other cytoskeletal proteins; 4 centrosomal proteins; 10 chaperons; 5 Golgi proteins; 7 mitochondrial proteins; 62 nucleic acid-binding proteins; 14 nuclear proteins; 13 ribosomal proteins; 28 vesicle transport proteins; 83 proteins with diverse function and/or localization; and 42 uncharacterized proteins (Fig. 4). This multiplicity implies that our present method is not specific for identifying only MAPs.